AFRL-RV-PS-
TR-2021-0002

AFRL-RV-PS
TR-2021-0002

ON THE STABILITY OF HIGH FREQUENCY WAVE REGIONAL AMPLITUDES: A STUDY OF MIDDLE EASTERN Q MODELS AND THEIR RELIABILITY

Eric Sandvol, et al.

University of Missouri
310 Jesse Hall
Columbia MO 65211

15 August 2020

Final Report

APPROVED FOR PUBLIC RELEASE; DISTRIBUTION IS UNLIMITED.

AIR FORCE RESEARCH LABORATORY
Space Vehicles Directorate
3550 Aberdeen Ave SE
AIR FORCE MATERIEL COMMAND
KIRTLAND AIR FORCE BASE, NM 87117-5776

DTIC COPY

NOTICE AND SIGNATURE PAGE

AFRL-RV-PS-TR-2021-0002 HAS BEEN REVIEWED AND IS APPROVED FOR PUBLICATION IN ACCORDANCE WITH ASSIGNED DISTRIBUTION STATEMENT.

//SIGNED//	//SIGNED//
Dr. Frederick Schult	Erin N. Pettyjohn, Chief
Program Manager, AFRL/RVBN	AFRL Geospace Technologies Division

REPORT DOCUMENTATION PAGE

Form Approved
OMB No. 0704-0188

1. REPORT DATE *(DD-MM-YYYY)*	**2. REPORT TYPE**	**3. DATES COVERED** *(From - To)*
15-08-2020	Final Report	21 Jul 2017 – 21 Jul 2020

4. TITLE AND SUBTITLE
On the Stability of High Frequency Wave Regional Amplitudes: A study of Middle Eastern Q models and their Reliability

5a. CONTRACT NUMBER
FA9453-17-C-0027

5b. GRANT NUMBER

5c. PROGRAM ELEMENT NUMBER
62601F

6. AUTHOR(S)
Eric Sandvol, Ayoub Kaviani, Rengin Gok, and Duyi Li

5d. PROJECT NUMBER
1010

5e. TASK NUMBER
EF130512

5f. WORK UNIT NUMBER
V148

7. PERFORMING ORGANIZATION NAME(S) AND ADDRESS(ES)
University of Missouri
310 Jesse Hall
Columbia, MO 65211

8. PERFORMING ORGANIZATION REPORT NUMBER

9. SPONSORING / MONITORING AGENCY NAME(S) AND ADDRESS(ES)
Air Force Research Laboratory
Space Vehicles Directorate
3550 Aberdeen Avenue SE
Kirtland AFB, NM 87117-5776

10. SPONSOR/MONITOR'S ACRONYM(S)
AFRL/RVBY

11. SPONSOR/MONITOR'S REPORT NUMBER(S)
AFRL-RV-PS-TR-2021-0002

12. DISTRIBUTION / AVAILABILITY STATEMENT
Approved for public release; distribution is unlimited (AFMC-2020-0593 dtd 23 Dec 2020)

13. SUPPLEMENTARY NOTES

14. ABSTRACT
The objective of this work is to understand the origin of relatively large variations in Lg amplitudes that do not appear to be a first order effect of path, station, or source. We have investigated this variance by improving existing attenuation models for the northern Middle East by combining important new data sets, specifically data from the Syrian, Iraqi, and Iranian national networks, using a Reverse Two Station approach with a minimal number of assumptions. In order to evaluate our ability to remove path based and site-based effects on high frequency amplitudes, we are working to measure the inherent variation in the regional phase amplitudes. We have chosen to focus on Lg amplitudes since they have the highest signal to noise ratio for continental paths) as well as coda throughout the northern Middle East. Furthermore, we are striving to understand the origin of this variance in order to more accurately predict direct phase amplitudes and also to understand the variance associated with each. We accomplished this by generating probability distributions of Q(f) for every reverse two station (RTS) path with a sufficient number of repeated paths. We have found a surprisingly large variation in RTS amplitude reduction. This result cannot be explained by variation in source radiation patterns or by site amplification terms (neglecting azimuthal variation), Q anisotropy, or complexity of the scattered wave field.

15. SUBJECT TERMS
seismic wave propagation, Q Tomography

16. SECURITY CLASSIFICATION OF:			**17. LIMITATION OF ABSTRACT**	**18. NUMBER OF PAGES**	**19a. NAME OF RESPONSIBLE PERSON**
a. REPORT	**b. ABSTRACT**	**c. THIS PAGE**			Dr. Frederick Schult
Unclassified	Unclassified	Unclassified	Unlimited	72	**19b. TELEPHONE NUMBER** *(include area code)*

This page is intentionally left blank.

Table of Contents

List of Figures

This page is intentionally left blank.

1. SUMMARY

We have worked to improve existing attenuation models for the northern Middle East by combining important new data sets, specifically data from the Azeri, Georgian, Iranian, and Iraqi national networks making a minimal number of assumptions using a Reverse Two Station approach. In order to evaluate our ability to remove path-based and site-based effects on high frequency amplitudes, measured the inherent variations in the Lg amplitudes as well as coda throughout the northern Middle East. We have focused our efforts on Lg because it has the highest signal to noise ratio for continental paths. We are working to understand the origin of this variance in order to more accurately predict direct Lg amplitudes and also to understand the variance associated with each. To address this we are generating probability distributions of Q(f) for every reverse two station (RTS) path with a sufficient number of repeated paths. We have found a surprisingly large variation in RTS amplitude reduction. This result cannot be explained by variation in source radiation patterns, in site amplification terms (neglecting azimuthal variation), or in Q anisotropy or complexity of the scattered wave field.

Over the past ten years we have worked to create physically based models of regional phase attenuation in the Middle East. Our objectives have been to isolate the path, site and source effect with the objective of effectively removing the site and path effects so that better source information can be extracted. We have utilized a restrictive path geometry that should effectively isolate source (even for an azimuthally varying source radiation pattern), isotropic site amplification, instrument response, and path. Despite this restrictive geometry and very few assumptions, we have been able to collect a large number of station pairs with over 50 repeated RTS paths. This critical mass of data give us insight into the stability of our Q models as well as the repeatability of the path-based attenuation. We are working to increase the number of repeated paths in order to better understand the factors that generate the large variation in the observed amplitude reductions for repeated paths. This is possible with the large number of contemporaneously recording stations from which we are collecting data in the region (Figure 1).

2. INTRODUCTION

We have collected broadband data from a wide variety of seismic stations across the Middle East (Figure 1). The majority of our stations are in the Northern Middle East and thus we have focused much of our effort on Reverse Two Station (RTS) paths across the Arabia-Eurasia plate boundary. These stations consist of both temporary and permanent stations that have been deployed over the past 25 years. These stations also have a wide range of sample rates and instrument responses; the instrument responses vary in reliability. Using RTS data we have been able to isolate and, in some cases, improve the instrument response data set that should help reduce the effect of incorrect instrument response data. This reliable instrument response data is critical as we have discovered that one of the best ways to isolate the cause of Lg amplitude instability is the Two Station Method (TSM). In total we have waveform data from approximately 500 stations in the region.

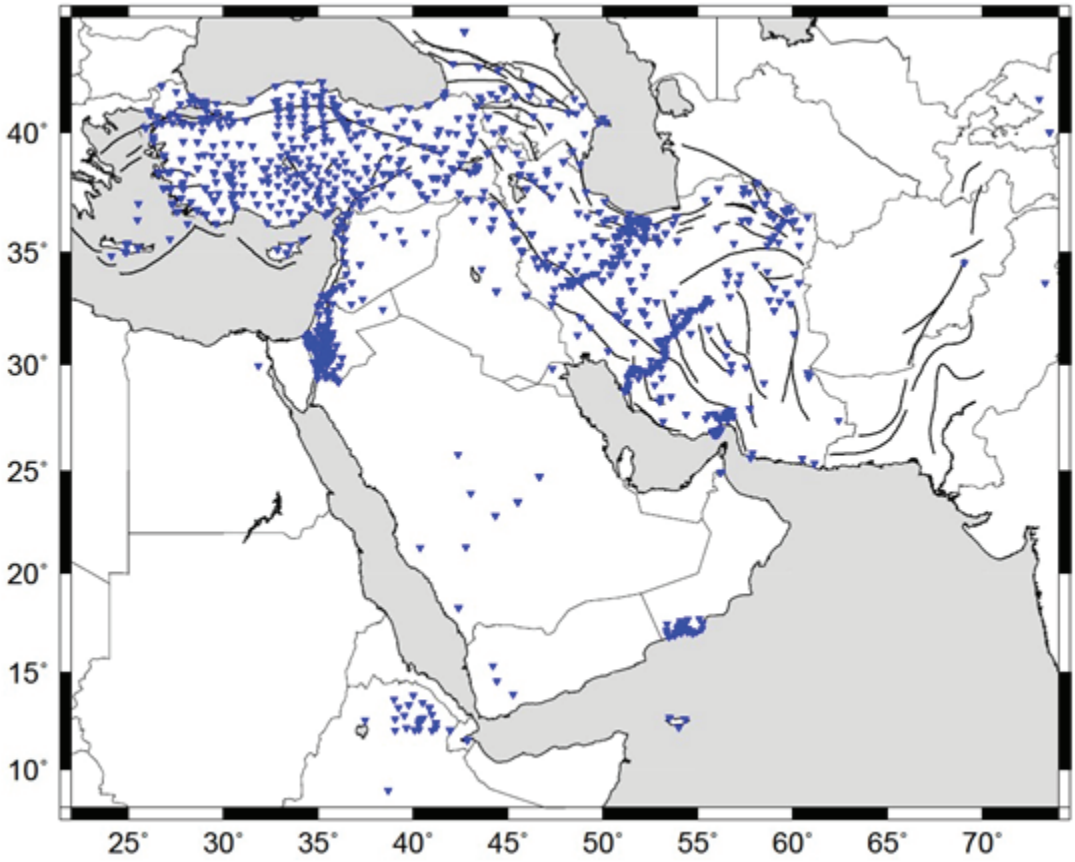

Figure 1. A regional map showing the new and existing stations that we have used to determine the stability regional phase amplitudes. *We now have very dense station coverage in both the Anatolian and Iranian plateaus. It is important to note that we have a large number of newly available stations especially within southern Russia, Georgia, Azerbaijan, and Armenia that greatly expand our RTS inventory.*

Given that the reverse two station paths should effectively eliminate source and site effects and that the path effects should be consistent, we initially investigated six possible effects that could possibly explain the variation in the RTS amplitude reduction:

1. Signal to noise not sufficient
2. Azimuthal variations in the path-based attenuation (likely scattering) within the +/-15° limit that defines our two station paths
3. Temporal variation in instrument response (particularly gain)
4. Source depth exciting different modes of Lg or Pg propagation
5. Azimuthal variation in site amplification
6. Contamination from one-way phase conversion (such as Sn-to-Lg conversion)

In general, we have an approach to isolate each of these effects, although azimuthally dependent site amplification presents the most challenging of these six options to isolate. Direct phase amplitudes seem to possess a certain level of inherent instability or

randomness that cannot be effectively modeled with a deterministic approach. In other words, we find that even after accounting for all of the possible effects, there is a significant variance in the behavior of high frequency amplitudes in certain parts of the Middle East. We can, however, quantify (see, for example, Figure 2) and map the variation in amplitude reduction using our large database of repeated RTS paths. We accomplish this by mapping the spatial structure of the remaining variance after correcting for effects 1-4 listed above.

In addition to studying direct phase amplitudes, we also measured the inherent uncertainty in coda across the Iranian and Turkish plateaus. We have used all of the same data from our work on Lg, Sn and Pg to measure different aspects of coda in order to construct a model for how coda parameters vary in two dimensions across the northern Middle East. This has allowed us to compare Q values obtained from source corrected amplitude spectra. In order to better characterize source characteristics to improve attenuation models, we used the empirical technique of Mayeda et al., 2003 and Gok et al., 2016, to measure coda parameters for the Iranian plateau.

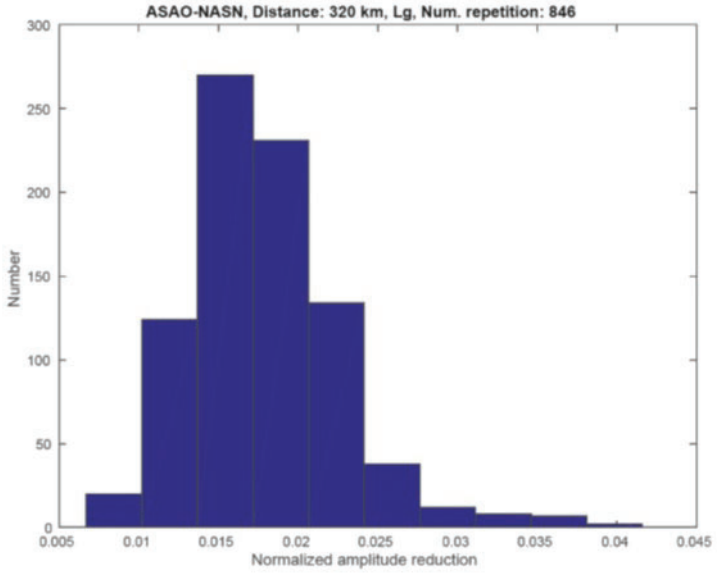

Figure 2. A histogram for a repeated reverse two-station path measurement for Lg amplitude reduction. *We have chosen this pair of stations because it generated the largest set of repeated RTS paths (846). This particular RTS path is for a station pair within the Iranian plateau. In theory, these repeated paths should always show exactly the same amplitude reduction for all of these paths, and yet we observe substantial differences in the observed amplitude reduction.*

As a part of this contract, we have compiled approximately 500 of these distributions for different station pairs across the Middle East (Figure 3). This is an example of the large inherent variation in amplitude reduction (and Q as well) for these repeated paths. This is a somewhat surprising result and cannot be explained by variation in source radiation patterns, in site amplification terms (neglecting azimuthal variation), or in Q anisotropy complexity of the scattered wave field. Nearly all of these effects should be removed by the RTS path geometry.

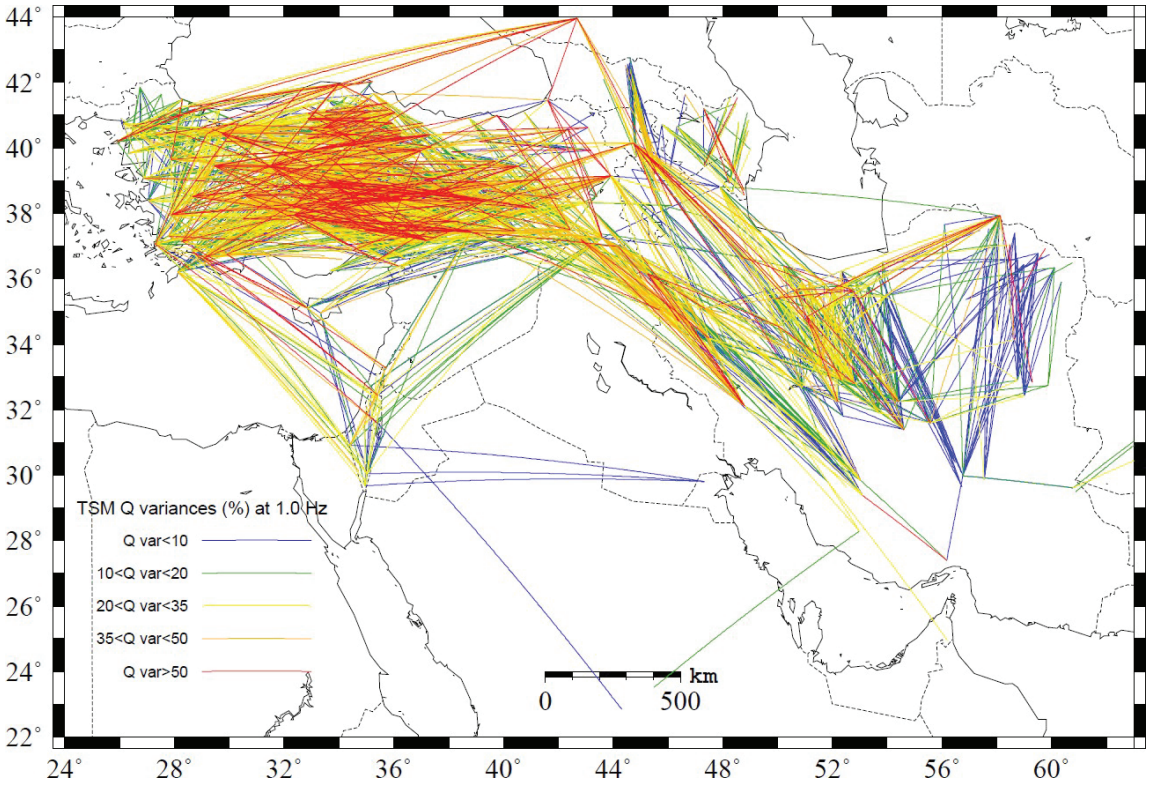

Figure 3. Error estimates using repeated paths for all TSM station pairs with at least 50 repeated paths at 1 Hz.

We have shown our final database for all repeated paths for TSM (Figure 3) and Reverse Two Methods (RTM) (Figure 4) paths. It is worth noting the large difference in the repeated path standard deviation of Lg Q for the TSM versus the RTM paths. This is consistent with the TSM paths being subject to assumptions about the consistency in site amplification and errors in the estimated instrument response.

Our primary goal for this contract was to isolate the primary causes of this large variation by exploring both temporal and azimuthal variation in the RTS repeated paths. The proposed research was only possible because we have managed to accumulate 220,000 reverse two-station paths covering the entire northern Middle East. We have expanded this data set to over 300,000 reverse two-station paths so that we can examine how different tectonic provinces and source types affect the RTS variation differently.

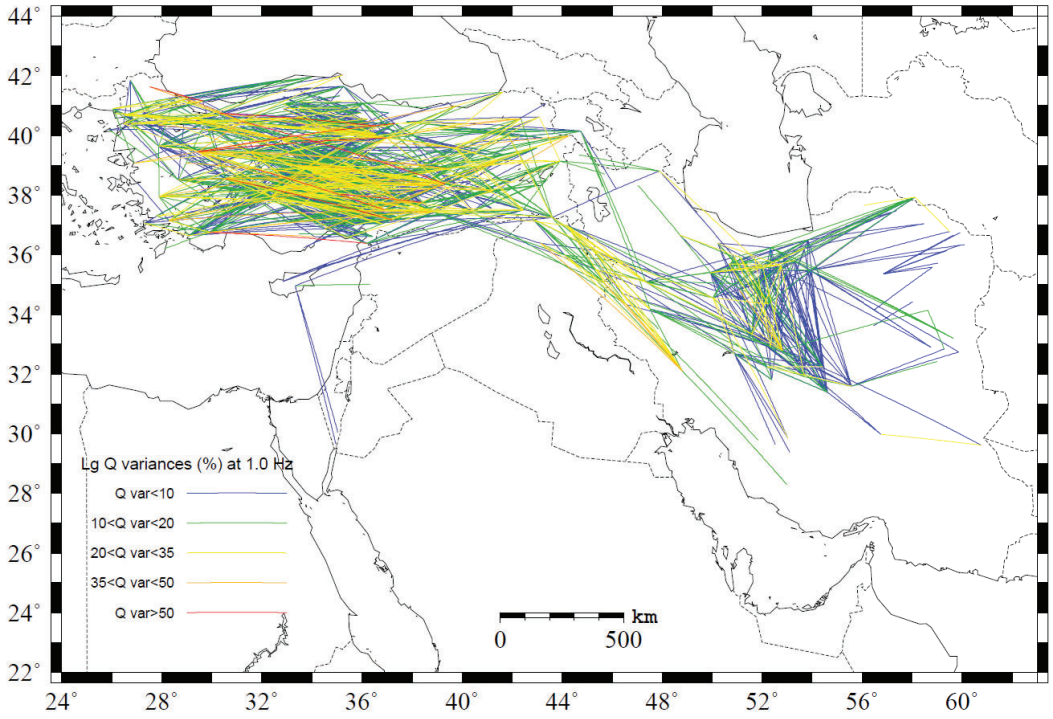

Figure 4. Error estimates using repeated paths for all RTS station pairs with at least 50 repeated paths at 1 Hz.

In order to better understand the spatial deviations in our repeated path estimates for both the TSM and RTS measurements, we tomographically mapped these variations (Figures 5 and 6) assuming a linear spatial dependence of the reciprocal of the relative Q uncertainty (uncertainty in Q divided by the mean Q value) which we briefly discuss in the method section. We can see that, as expected, the TSM uncertainty estimates are about twice as large as the RTS uncertainty estimates. This is consistent with the theoretical difference between RTS and TSM estimates in Q and with what to some degree has been shown in other studies, the best example being Ford et al. (2008). What is more interesting is where we see the large uncertainties. We observe that in both the TSM and RTS models, the largest uncertainties are in regions where the Sn propagation is most efficient (westernmost Turkey and the Zagros), although these regions are at the edge of the RTS model where resolution is poorer. Comparisons of the TSM and RTS uncertainties in eastern Turkey are interesting because we see large uncertainties for the TSM Q model but relatively low uncertainties for the RTS values. This could suggest relatively large variation in site terms for station pairs in this region.

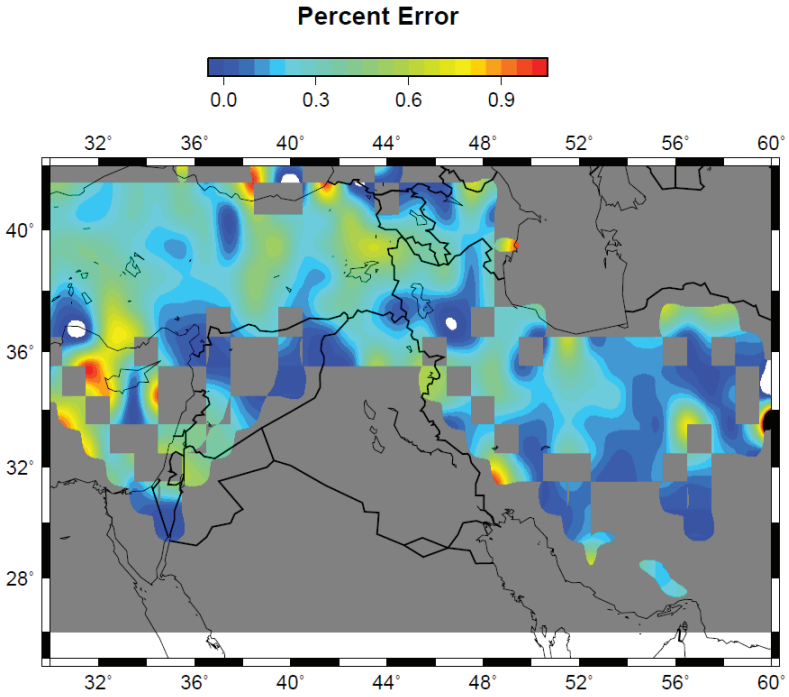

Figure 5. A tomographic projection of the TSM repeated path estimates of Lg Qeff uncertainty. *This gives us a better idea of the spatial variations in TSM uncertainty than color-coded ray path plots. The large values are located in regions where Sn waves are efficient.*

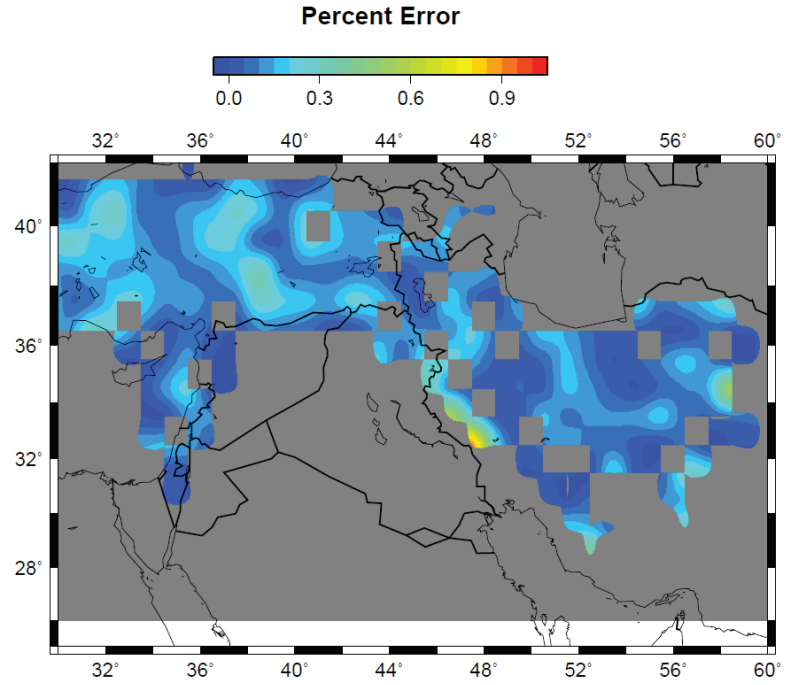

Figure 6. A tomographic projection of the RTS repeated path estimates of Lg Qeff uncertainty. *This gives us a better idea of the spatial variations in RTS uncertainty. than color-coded ray path plots. Note how much smaller the uncertainty estimates are compared with the TSM model in Figure 5.*

One of the possible explanations for the large instabilities in Lg Q shown in Figure 3 is that relatively small variations in azimuth may lead to large changes in the amplitude reductions between any two given seismic stations. This kind of strong azimuthal change could be generated by strong azimuthally dependent scattering of the Lg and Pg

wavefields. In order to test this idea, we have looked at the variance reduction, assuming a Gaussian distribution, when reducing the allowable azimuthal variation between the two events' back-azimuths and the azimuth between two stations. We have typically allowed a +/- 15-degree variation. We have enough RTS repeated paths that we can reduce this to +/- 6 degrees and still have a relatively large number of RTS paths. If the path azimuth were largely responsible for the Lg amplitude instability, we would expect to see a large variance reduction when using a 6-degree azimuthal variation. Instead, we observe almost no change in Lg Q variance (Figure 7). This result strongly suggests that azimuthal variation is not responsible for the large instabilities we observe in Figure 3. We have systematically examined the effect of source distance and depth on Lg amplitude instabilities.

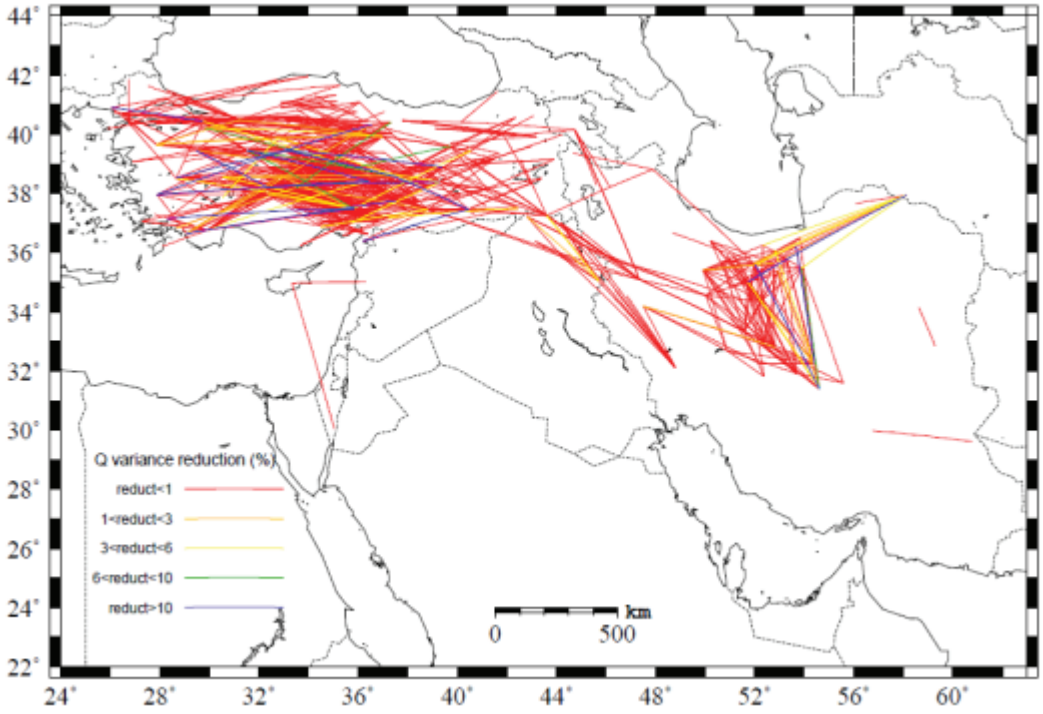

Figure 7. A map showing the difference in the standard deviations for a 15- and 6-degree difference in the azimuth between two events for all RTS pairs. *This shows that the Q stability is not a function of azimuth.*

Given that the reverse two station paths should effectively eliminate source and site effects, the path effects should be very consistent (see Kaviani et al. 2015). We therefore began by studying six possible effects, below, that could possibly explain the variation in the RTS amplitude reduction (an example for this in the lower frequency band is shown in Figure 6). It is worth noting that we have now largely ruled out most of these six items as major contributors to Lg amplitude instability.

1. Signal to noise not sufficient
2. Azimuthal variations in the path-based attenuation (likely scattering) within the +/- 15° limit that defines our two station paths
3. Temporal variation in instrument response (particularly gain)

4. Source depth exciting different modes of Lg or Pg propagation
5. Azimuthal variation in site amplification
6. Contamination from one-way phase conversion (such as Sn-to-Lg conversion)

Because we have some evidence that most, if not all, of our original six possible reasons are not proving to be the source of the instabilities, we considered some other possible contributors:

7. Epicentral distance leading to different Lg propagation characteristics
8. Processing of Lg amplitudes: RMS versus frequency domain calculation of amplitude
9. Combination of depth and distance leading to different propagation modes.

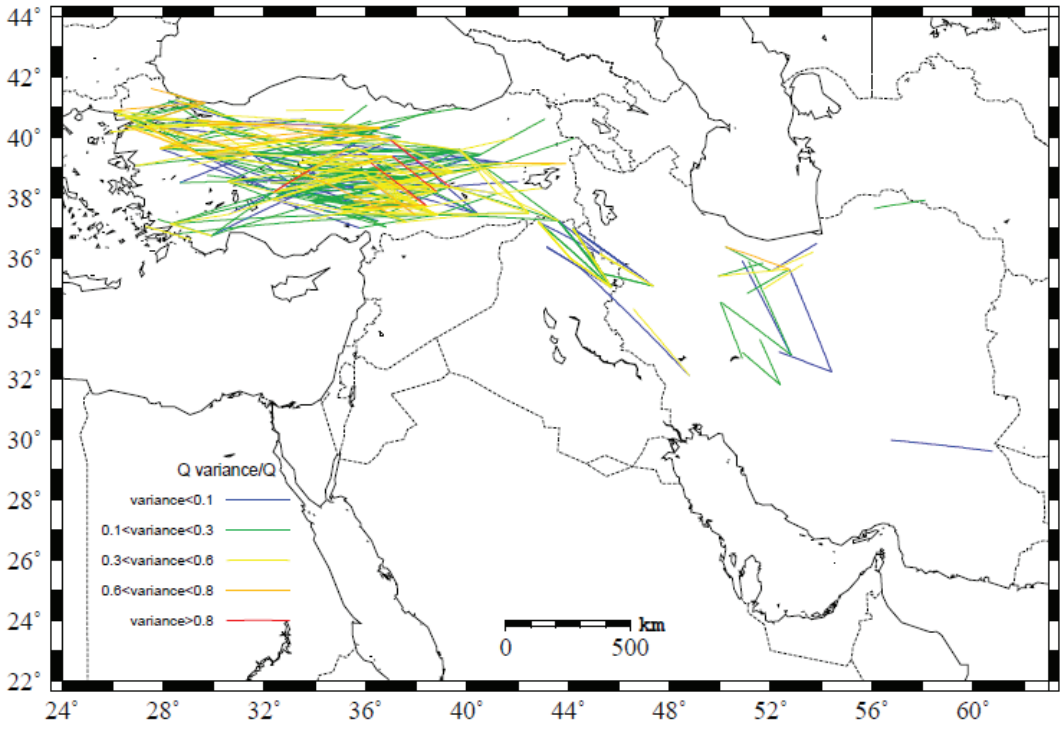

Figure 8. A plot of Reverse Two Station Method (RTSM) paths and the percentage variance in amplitude change for the frequency band 0.5 to 1.0 Hz.

In general, we continued our initial methods to isolate item #7. It is also quite straightforward to change the way we calculate regional phase amplitudes (#8) to see whether anything in our processing might cause these instabilities. We approach #9 as a multi-variate statistical problem to see whether a combination of depth and distance could generate more instability.

On a related note, we have examined the frequency dependence of variations in repeated path RTSM Q estimates. In general, we see very little frequency dependence to the Lg Q instability. Figure 8 shows the variance in the amplitude reduction (change in amplitude from the nearest station to the farthest station) for RTSM paths within central Turkey for the 0.5 to 1 Hz frequency band. We see a similar amount of

variation/instability in the amplitude reductions as we see for other frequency bands: 0.5 to 1 Hz, 1.0 to 1.4 Hz, 1.4 to 1.8 Hz, 1.8 to 2.2 Hz, and 2.2 to 2.6 Hz. In all of these frequency bands, we see very little difference in the distribution of repeated path RTSM Q values (or amplitude reductions).

3. METHODS USED TO ESTIMATE CHANGE IN EFFECTIVE Q AND VELOCITY

In order to determine which of the potential causes for regional phase amplitude instability listed in the introduction of this report are significant, we investigated the original six. In this section we explain the methods we are using to isolate the key remaining factors influencing Lg Q stability. We recognize that much of this description of the two station (TSM), reverse two station (RTS), and double two station (DTSM) methods has been included in our earlier reports, but we include it in our final report for the sake of completeness.

3.1 Review of Two Station and Reverse Two Station Methods

The amplitude of a seismic wave may be described by an exponential attenuation equation that accounts for both geometric spreading and attenuation,

$$A(\omega) = I(\omega)E(\omega)S(\omega)G(\Delta)\exp\left\{\frac{\pi f \Delta}{vQ(f)}\right\} \qquad (1)$$

where A is the observed amplitude between source and receiver for a wave of period t recorded at distance Δ. Here, I is the instrument response, E is the source amplitude, S is the site amplification response, and v is the wave group speed. Geometric spreading (G) is described by a frequency independent exponent. For cylindrical spreading, the exponent should be 0.5, and for spherical spreading, itis 1.0. When dispersion is accounted for, these can increase by up to 0.3 depending on signal bandwidth. Spreading relations are important but poorly documented and must be given explicit attention in attenuation problems. The attenuation quality factor, Q, can be assumed to be frequency dependent, $Q=Q_0 f^{\eta}$ with Q_0 being the attenuation quality factor at 1 Hz, f the wave frequency, and η describing the frequency dependence. Values for Q_0 and η depend on the type of wave used but generally η lies between zero and one. This equation does not account for radiation pattern, focusing, or anisotropic effects. However, with good azimuthal coverage, these effects should average out. Both Q and amplitude tomography methods are based on this equation, with appropriate modifications.

The TSM was presented by Mitchell (1995) and has been widely used (e.g., Nuttli, 1980). Xie and Mitchell (1990) used this assumption in the TSM:

$$(1-\eta)\ln f - \ln Q_0 = \frac{v}{\pi(d_j - d_i)}\ln\left(\frac{A_i(f)I_j(f)d_i^m}{A_j(f)I_i(f)d_j^m}\right). \qquad (2)$$

The real situation for applying the TSM is more complicated because the perfect alignment geometry is typically not obtainable, especially for passive seismic experiments. In practice

the paths are different by a small angle $\delta\theta$. A detailed analysis of this angle has been presented by Xie et al. (2004). Systematic errors could be introduced into Q_0 and η values solved by the TSM because of effects of the attenuation caused by out of the path and anisotropic source radiation patterns. These errors can be minimized if a threshold value $\delta\theta_{max}$ is used to limit the angle $\delta\theta$. Xie et al. (2004) used a $\delta\theta_{max}$ of ±15° in their study, which had been estimated by Der et al. (1984). Xie et al. (2004) also derived an equation to minimize an error related to the variation of inter-station distance (especially, the contribution of variations of T_{FD}) at 1 Hz. This equation (A14 in Xie et al., 2004) is reorganized here:

$$\frac{\delta Q_0}{Q_0^2} = \frac{v}{\pi}\frac{1}{\left(d_j - d_i\right)}\delta x\,. \tag{3}$$

where d_j-d_i denotes the inter-station distance, and δQ_0 and δx errors in the measured Q_0 and associated with three-dimensional Earth structure. Equation 3 tells us how large the error of Q_0 is acceptable while only the δx smaller than 0.4 has been proved to be valid (Xie, 2002), which gives us a maximum error of Q_0 of approximately 0.4 when Q_0 is nearly equal to the inter-station distance. To reduce the error of Q_0, the inter-station distance should be as large as possible.

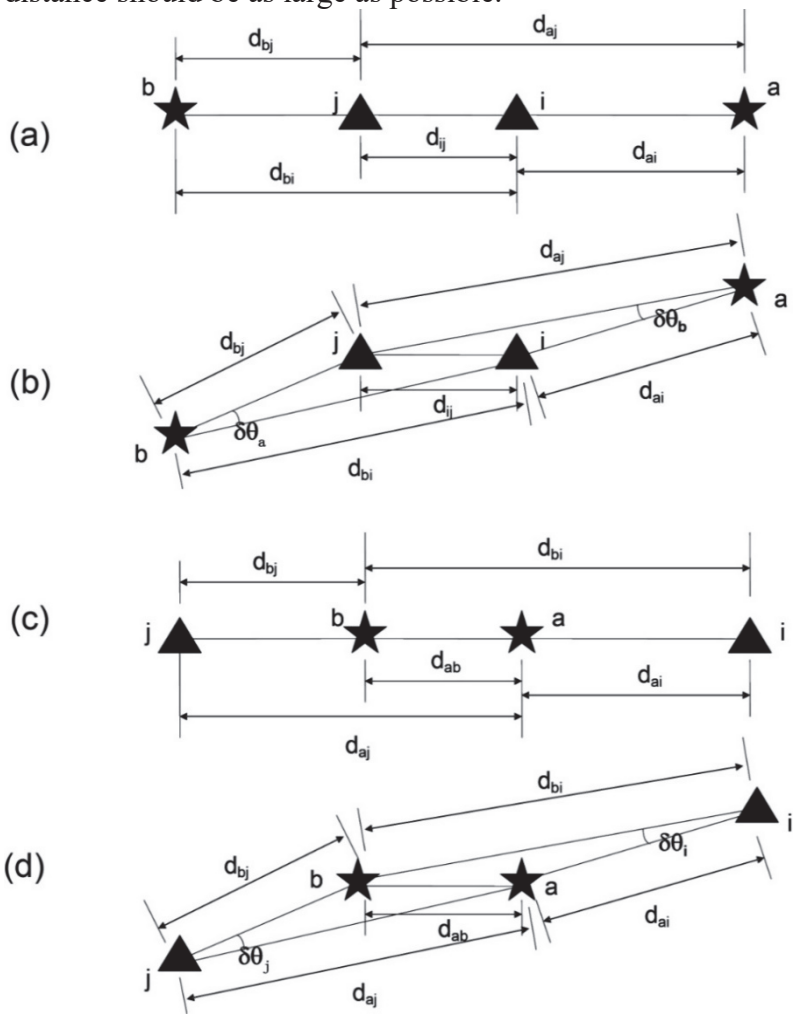

Figure 9(a) and (b): Schematic drawing of the geometry of RTS including (a) the ideal situation where source *a* (star on the right), stations *i* and *j* (triangles), and source *b* (star on the left) are aligned along a great circle, and (b) the more realistic situation where the azimuth difference angles of sources *a* and *b* are denoted by $\delta\theta_a$ and $\delta\theta_b$ respectively. (c) and (d): Schematic drawing of the geometry of RTE including (c) the ideal situation where station *i* (triangle on the right), sources *a* and *b* (stars), and station *j* (triangle on the left) are aligned along a great circle, and (d) the more realistic situation when the azimuth difference angles of station *i* and *j* are denoted by $\delta\theta_i$ and $\delta\theta_j$ respectively.

As can be seen in Figures 3 and 5, a significant disadvantage of the TSM is caused by the reserved instrument response I and neglected site response S_S. The instrument responses are only theoretically identical for stations with identical seismometers and data loggers. In reality, an instrument calibration is commonly impossible during its deployment. It is difficult to guarantee the operability of calibration of all instruments. The site effects are known to have strong lateral variation and are likely associated with shallow geological structures especially in tectonically active zones (Wald and Allen, 2007; Meunier et al., 2008; Pasyanos et al., 2009). It is also worth noting here that equation 3 is the basis for our estimates of the spatial variation in the relative uncertainty in Lg Q (uncertainty in Q divided by the mean Q value).

The RTM was employed in order to avoid the effects of neglected S_S terms and inaccurate I terms in the TSM by involving one more event. The RTM was initially developed by Chun et al. (1987). Figure 9 shows the geometry of the RTM including its two cases: the Reverse Two Station (RTS) paths and Reverse Two Event (RTE) paths. The ideal case for RTS is that both events are aligned with the inter-station path, and the four epicentral distances involved are within a regional distance range. In such a situation, we use A_{ai}, A_{aj}, A_{bi}, and A_{bj} to denote spectral amplitudes of Lg recorded at stations i and j for events a and b, and d_{ai}, d_{aj}, d_{bi}, and d_{bj} the corresponding distances. The four spectra amplitudes can be expressed as:

$$\begin{cases} A_{ai}(f,d_{ai}) = S_a(f)R_a(f,\varphi)I_i(f)S_{Si}(f)G_{ai}(d_{ai})e^{-\frac{\pi f d_{ai}}{v_i Q_i}} \\ A_{aj}(f,d_{aj}) = S_a(f)R_a(f,\varphi)I_j(f)S_{Sj}(f)G_{aj}(d_{aj})e^{-\frac{\pi f d_{aj}}{v_j Q_j}} \\ A_{bi}(f,d_{bi}) = S_b(f)R_b(f,\varphi)I_i(f)S_{Si}(f)G_{bi}(d_{bi})e^{-\frac{\pi f d_{bi}}{v_i Q_i}} \\ A_{bj}(f,d_{bj}) = S_b(f)R_b(f,\varphi)I_j(f)S_{Sj}(f)G_{bj}(d_{bj})e^{-\frac{\pi f d_{bj}}{v_j Q_j}} \end{cases}. \quad (4)$$

If A_{ai} is divided by A_{aj} and A_{bi} is divided by A_{bj}, we get

$$\begin{cases} \frac{A_{ai}}{A_{aj}} = \frac{S_a}{S_a}\frac{R_a}{R_a}\frac{I_i}{I_j}\frac{S_{Si}}{S_{Sj}}\frac{G_{ai}}{G_{aj}}\exp\left(\frac{\pi f d_{aj}}{v_j Q_j} - \frac{\pi f d_{ai}}{v_i Q_i}\right) = \frac{I_i}{I_j}\frac{S_{Si}}{S_{Sj}}\frac{G_{ai}}{G_{aj}}\exp\left(\frac{\pi f d_{aj}}{v_j Q_j} - \frac{\pi f d_{ai}}{v_i Q_i}\right) \\ \frac{A_{bi}}{A_{bj}} = \frac{S_b}{S_b}\frac{R_b}{R_b}\frac{I_i}{I_j}\frac{S_{Si}}{S_{Sj}}\frac{G_{bi}}{G_{bj}}\exp\left(\frac{\pi f d_{bj}}{v_j Q_j} - \frac{\pi f d_{bi}}{v_i Q_i}\right) = \frac{I_i}{I_j}\frac{S_{Si}}{S_{Sj}}\frac{G_{bi}}{G_{bj}}\exp\left(\frac{\pi f d_{bj}}{v_j Q_j} - \frac{\pi f d_{bi}}{v_i Q_i}\right) \end{cases}. \quad (5)$$

Like the TSM, we assume that the velocity structure is one-dimensional and apparent Q values are identical at stations i and j. We divide the two ratios in (5), substitute, and obtain

$$\frac{A_{ai}A_{bj}}{A_{aj}A_{bi}} = \left(\frac{d_{ai}d_{bj}}{d_{aj}d_{bi}}\right)^{-m} \exp\left[\frac{\pi f}{vQ}\left(d_{aj} - d_{ai} - d_{bj} + d_{bi}\right)\right]. \quad (6)$$

Therefore, the inter-station (between *i* and *j*) apparent $1/Q$ value can be derived as

$$\frac{1}{Q} = \frac{v}{\pi f\left(d_{aj} - d_{ai} - d_{bj} + d_{bi}\right)} \ln\left[\frac{A_{ai}A_{bj}}{A_{aj}A_{bi}}\left(\frac{d_{ai}d_{bj}}{d_{aj}d_{bi}}\right)^{m}\right], \quad (7)$$

whose reciprocal is the inter-station apparent Q. Like the TSM, (4) to (7) are all in the frequency domain. The $1/Q$ as a function of the frequency f is

$$\frac{1}{Q(f)} = \frac{v}{\pi f\left(d_{aj} - d_{ai} - d_{bj} + d_{bi}\right)} \ln\left[\frac{A_{ai}(f)A_{bj}(f)}{A_{aj}(f)A_{bi}(f)}\left(\frac{d_{ai}d_{bj}}{d_{aj}d_{bi}}\right)^{m}\right]. \quad (8)$$

Equation (8) shows that the RTS does not require any assumptions about the instrument or site responses. (8) is similar to (10), but it requires four spectra and four distances, not the two spectra and two distances in the TSM. A pre-determination of m is also required, like the TSM.

Tomographic inversions generally use least squares algorithms such as LSQR (Paige and Saunders, 1982). Constraints on the problem are of great importance and can be introduced using regularization and damping techniques. For example, spatial variations in attenuation are regularized using first or second difference smoothing constraints. Source models, such as MDAC (Magnitude and Distance Amplitude Correction; Walter and Taylor, 2001), can also be included in tomographic inversions for Q. Moments and corner frequencies can be damped to known levels for special events, or regularized to follow a best-fit scaling model (Phillips et al., 2009). Resolution and covariance are quantified using impulse responses, checkerboard tests, and matrix inversion techniques. Such estimates assume that the model equations describe the physics perfectly, which we know is not completely true. Dense networks such as the Iranian combined networks have allowed us to investigate what are very often unmodeled effects, such as the source radiation, focusing, and medium anisotropy effects mentioned earlier.

3.2 Estimation of Differential Q and V (ΔQv)

We have developed empirically based Q models and associated variances using much stricter azimuthal variation limits for RTM and TSM paths (10° and 5°, respectively). We tested azimuthal dependence for both our Two Station (TSM) and RTS Q measurements using two approaches: (1) evaluating the sensitivity of Q models using different azimuthal ranges and (2) looking at different probability distributions for different azimuthal ranges ($\delta\theta$ in Figure 10). These two approaches have given us an idea of the spatial variation in the effect of varying the limits of $\delta\theta$. This is only possible with a large database of contemporaneous paths.

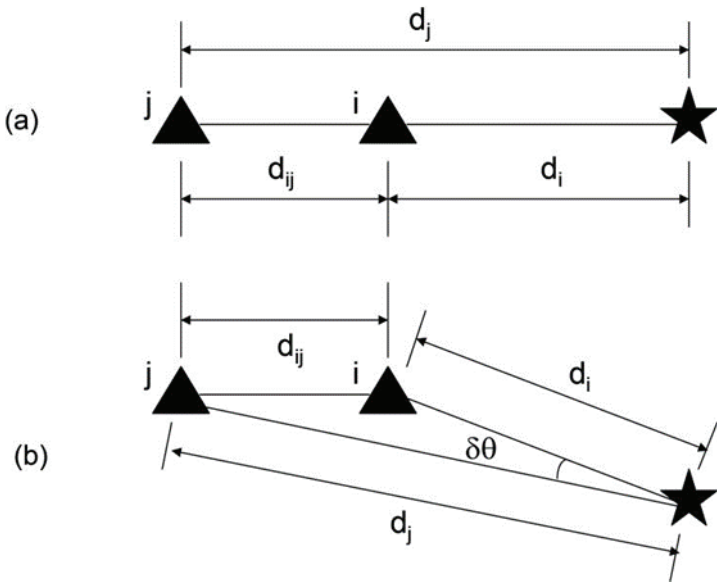

Figure 10. (a) An ideal recording geometry for the application of TSM for Q measurement. (b) A more realistic geometry in which the source-to-station azimuths vary by an amount $\delta\theta$.

We used the following approach to measure the effect of depth on the Lg Q (e.g. Baker et al., 2004). If we modify the RTM approach shown in equation 8 such that we use two events, each with substantially different hypocentral depths, on the same side of any given two station pair we can isolate by taking the ratio of the two TSM amplitude ratios, giving us:

$$R^{FS} = \frac{A_1^1}{A_2^1}, R^{FD} = \frac{A_1^2}{A_2^2}, \quad \frac{R^{RD}}{R^{FS}} = \frac{G(\Delta_2^1)G(\Delta_1^2)}{G(\Delta_1^1)G(\Delta_2^2)} \cdot \exp -\pi f \Delta_i \left[\frac{1}{V_D Q_D} - \frac{1}{V_S Q_S} \right], \quad (9)$$

$$where \ \Delta_i = \Delta_1^1 - \Delta_2^1 = \Delta_1^2 - \Delta_2^2$$

The superscript is the source index and the subscript is the station index. RFS and RFD are the amplitude ratios for the shallow and deep source respectively while QS and QD are the Q values for shallow and deep sources. This geometry is illustrated in Figure 11. Note that similar to the RTM method, the DTSM eliminates both the source and isotropic site amplification contributions to the amplitudes, thus isolating the geometric spreading and path-based attenuation. The geometric spreading function also becomes unity when the epicentral distances are the same. Even for epicentral differences for the far station as great as 20% of the average epicentral distance, this function will be within 6% for a geometrical spreading coefficient of 1 and 3% for a spreading coefficient of 0.5. Furthermore, we can determine whether there is a distance dependence to the DTSM values to understand whether there is any distance dependence to the DTSM differential reciprocal Q values.

We can re-write the difference in the reciprocal of the product of Q and V shown in equation 2 by introducing a ΔQV and using estimates of mean QV taken from the RTS estimates:

$$\Delta QV = V_S Q_S - V_D Q_D = (QV)^2 \pi f \Delta_i \log(R^{RD}/R^{FS}) \quad (10)$$

The mean values of Q and the Lg velocity are taken from measurements of RTSM Q and velocity measurements of the Lg velocity window. For equation 3 we have assumed that the geometrical spreading terms have become unity. We have chosen this approach to characterize variations in amplitude reductions because ΔQV terms can more easily be related to Q models than to the differences in the reciprocal of QV terms.

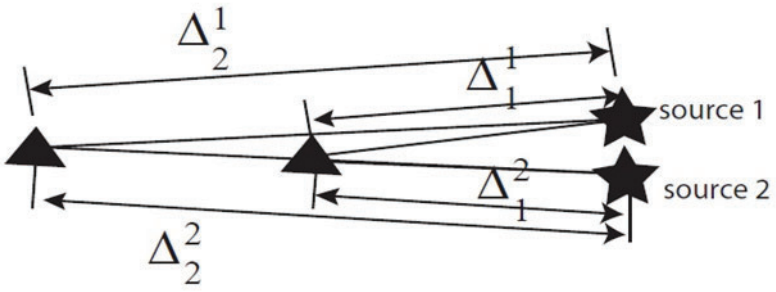

Figure 11. A schematic illustration of the Double Two Station Method's (DTSM) geometry with the distances shown in Equation 2.

We are using this approach to systematically isolate the effect depth of seismic attenuation and velocity. It is important to note, however, that this approach does not necessarily allow us to separate these two factors. We can use this approach to test how differential QV changes as a function of relative changes in hypocentral depth. One can see from Equation 2 that when QD = QS and the epicenters of the two events are identical, this ratio becomes unity. We can also compare our results from this approach to the comparison of combinations of different RTSM measurements using different depth values.

In addition we have used equation 9 and the DTSM method to explore the distance effects as well. The approach is the same only we use sources that are located at some distance apart. By using events with different epicentral distances but, on the same side of any given two station pair, we can isolate the differential Q by taking the ratio of the two TSM amplitude ratios:

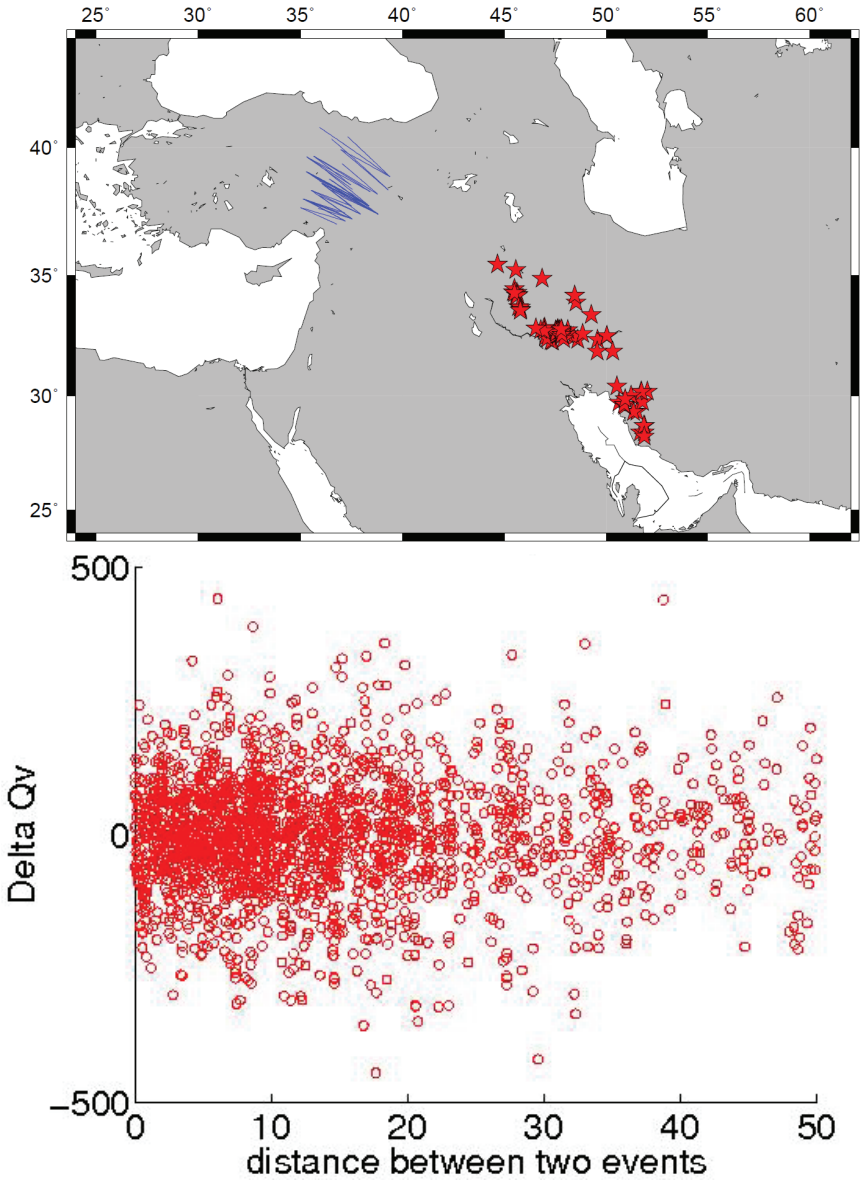

Figure 12. A plot of ΔQV for a particular two station pair located within the Iranian plateau. *The mean of these measurements is very close to zero, although slightly biased in the positive direction. The sign of ΔQV indicates whether the bias in the amplitude reductions is in the reverse or forward direction with respect to these two stations.*

Using this same approach then the two subscripts become the two events with different distances on either side of a two-station pair. An example is shown in Figure 12. The superscript 1 would be for the near event and 2 is for the more distant event.

$$\Delta QV = \frac{V_2 V_1 Q_2 Q_1}{Q_1 V_1 - Q_2 V_2} \tag{11}$$

The mean values of Q and the Lg velocity are taken from measurements of TSM Q and velocity measurements of the Lg velocity window for the entire paths. For equation 3 we have assumed that the geometrical spreading terms have become unity; in other words, we have assumed no changes in the geometrical spreading coefficient. We have chosen this approach to characterize variations in amplitude reductions because ΔQV terms can more easily be related to Q models as opposed to the differences in the reciprocal of QV terms. The meaning of the subscripts in equation three depend upon the nature of the differences in source parameters we are testing. If we are testing the effect of source depth, then the subscripts would refer to the deep and shallow relative source depths as we have shown in equation 2. However, if we are exploring the difference in epicentral distance then the subscripts refer to the near event (indices 1) and far event (indices 2). The variations as a function of distance for the reciprocal of QV (Δ{1/QV}) in equation 2 appear to behave in very similar ways to differences in QV.

We have studied the sources of the repeated Reverse Two Station (RTM) measurements of Lg Q which effectively eliminate source and site effects. We have been able to quantify the stability and reliability of high-frequency Lg attenuation. We notice that for many regions, Lg amplitudes can be quite unstable, leading to large uncertainties in estimates of Lg Q(f).

We observe some weak distance dependence in ΔQV for distances out to 1000 km. We do not observe any structure to the distance dependence of ΔQV for events located within 50 kilometers of one another. It is somewhat surprising that even for events within 5 kilometers of each other, there is no systematic reduction or increase in ΔQV. It may also be that absolute distance is more important in the behavior of ΔQV.

Another part to this contract is looking at the stability of coda amplitudes. We have analyzed the stability of coda amplitudes by applying the same sensitivity tests using the same data that we have used on the direct amplitude data. We examined two station coda amplitude (TSCA) changes between three stations in the Iranian plateau. In general, we observe at least as much instability in the coda amplitude changes as we see in the direct wave amplitudes. This is a rather surprising result and one we must explore further with much larger data sets.

4. RESULTS

4.1 Greater Caucasus Data Set and Attenuation

One key aspect of the work on this contract is our work to expand the available contemporaneous data that is needed to create a large catalog of repeated RTS and TSM paths (Figure 13), including data from the Caucasus Seismic Network (CNET) (Figure 13). We analyzed 2,382 waveforms from 83 events occurring between 2017 and 2018 that were recorded at 97 stations in CNET. The event and station distributions are shown in Figure 13.

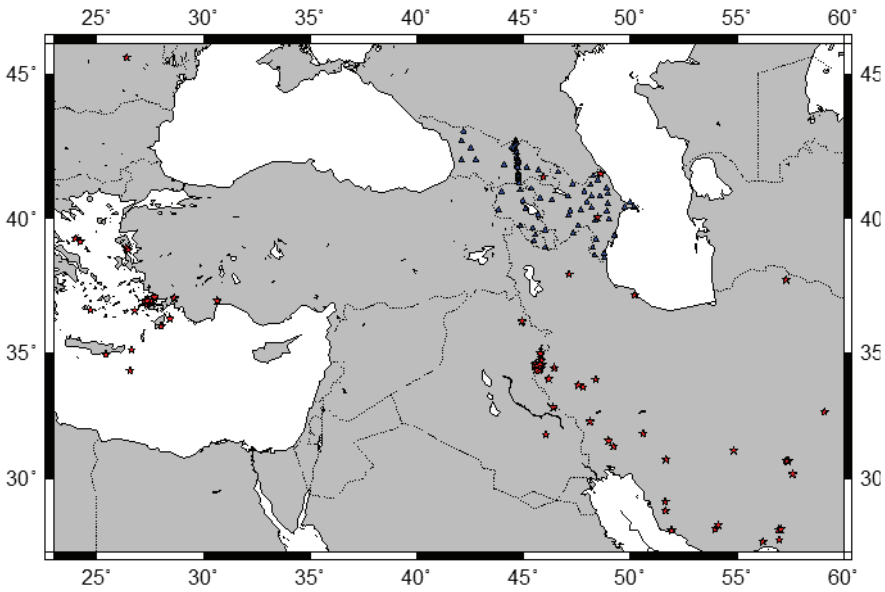

Figure 13. Events (red stars) and stations (blue triangles) used to study Lg attenuation across the Caucasus. *Nearly all of these stations were added during the period of the contract.*

Our data pre-processing consists of the following steps: (1) remove mean and trend of the seismogram; (2) automatically calculate Pn and Sn phase and manually re-pick Pn for correction; (3) automatically calculate the Lg window with a starting velocity of 3.5 km/s and an ending velocity of 2.9 km/s and manually re-pick the Lg using a starting velocity from 3.3 km/s to 3.7 km/s and a fixed velocity window with 0.6 km/s; and (4) compare the Lg energy with Pn and Pg energy to determine the Lg efficiency for the seismogram. Figure 14 shows that there is a great deal of overlap in the blocked and efficient Lg paths across and around the Greater Caucasus mountains at the northern edge of the Eurasia-Arabia collisional belt. This indicates a complex pattern of attenuation in this region. In order to understand the spatial variation in effective Lg Q, the study area is divided into 0.75°×0.75° cells to generate tomographic models of the TSM Q at 0.5 Hz and 1.0 Hz. Only station-pair paths with efficient or inefficient Lg at the near source station are used. Figures 14 and 15 show the ray path coverage and tomographic map, respectively, for the Lg Q model at 0.5 Hz. The tomography is based on 1,141 TSM measures over 502 paths. The ray path coverage can be used to resolve lateral variation in Lg Q from eastern

Armenia to central Georgia and eastern Azerbaijan. The Q values at 0.5 Hz in these areas are quite low, ranging between 50 and 150.

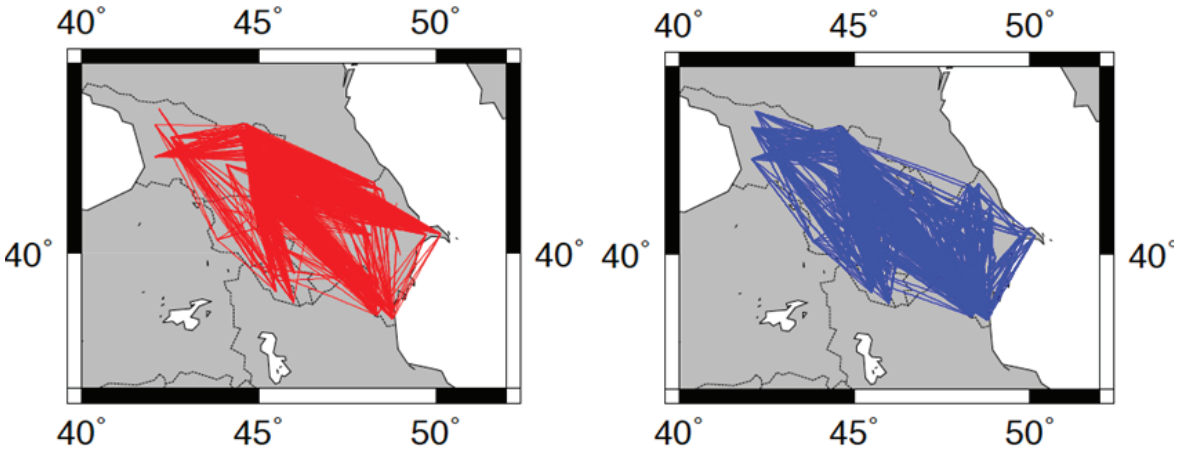

Figure 14. (Left; red) Blocked paths. (Right; blue) Efficient paths. *Note the similarity in paths.*

The low Lg Q_0 below 150 from central Armenia to Georgia suggests extremely strong crustal attenuation in this area (Figure 15), which correlates with high Moho temperature (Motavalli-Anbaran et al., 2016). Partial crustal melting and volcanism could be responsible for the crustal attenuation in this region. Considering that most of the events used are in the Iranian Plateau and Zagros Mountain belts, the rapid changes in crustal thickness should also play a role in the Lg attenuation in this region. As to the low Q_0, around 200, in eastern Azerbaijan, there is no evidence of hot crust or rapid Moho depth changes. The Lg attenuation here may be related to the relatively thick sediments in the Kura basin.

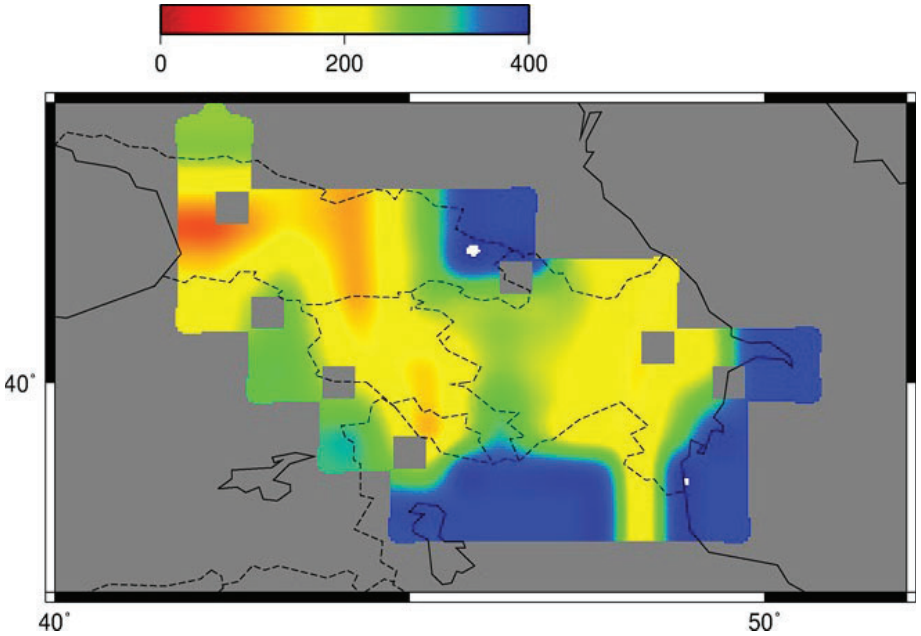

Figure 15. Caucasus Lg Q tomography at 0.5 Hz using the new data from our recently deployed Caucasus Network (CNET).

One explanation for the complexity in blockage we observe can be understood by looking into some of the details in propagation. We find that besides blocked and efficient station-pair paths, there are also station-pair paths with blocked Lg at the near source station but inefficient/efficient Lg at the far station. Because the Lg is already blocked near the source along its propagation path, it could be interpreted that the Lg at the far station comes only from energy focusing due to velocity variation. Figure 16 shows all the blocked-efficient paths of this type, where red represents the blocked half of the station pair path and blue represents the efficient/inefficient half. We can see a clear focusing trend from northern to southeastern Georgia and a small focusing area in central Armenia, which corresponds to the high S-wave velocity anomaly pattern starting at 20 km (Zabelina et al., 2016). This observation may be a result of Lg site amplification, but it is difficult to go from blocked to efficient Lg with only differential site amplification.

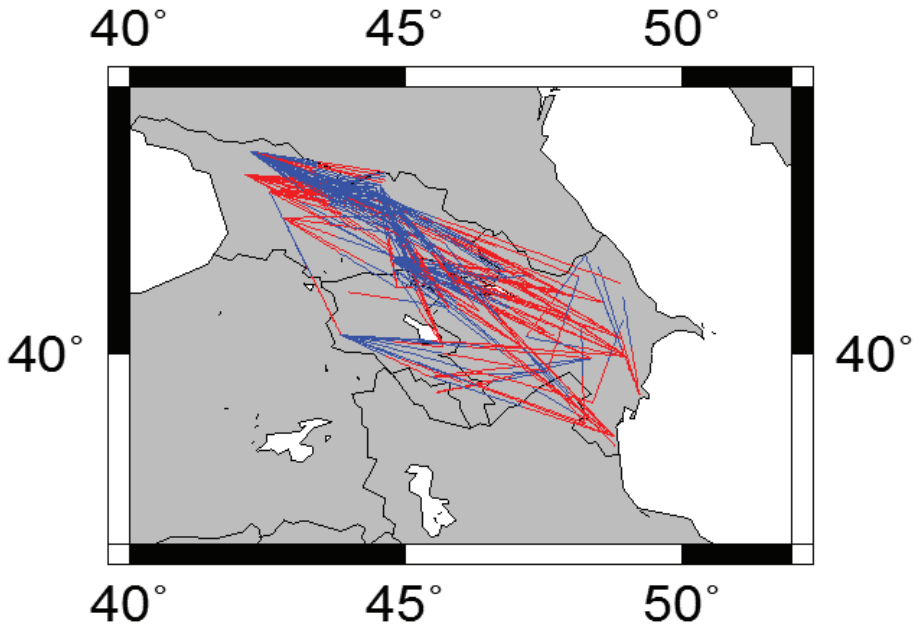

Figure 16. Blocked-efficient path distribution. *The red paths are the blocked half and the blue path are the efficient/inefficient half.*

Figure 17 and 18 show the results of combining our new and old Lg Q estimates. These new data show a shift in the position of the lowest Q zone in eastern Turkey. The very low Lg Q_0 from central Armenia to Georgia suggests extremely strong crustal attenuation in this area, which correlates with high Moho temperature estimates (Motavalli-Anbaran et al., 2016). There is also some correlation between this very low crustal Q and young volcanism, although there are some volcanic centers in eastern Turkey with Lg Q that is not as low. Given the relatively low Lg Q across the Iranian Plateau and Zagros Mountain belts, the rapid changes in crustal thickness should also play a role in Lg attenuation. Also, the low Q_0, around 200, in central Anatolia is consistent with young volcanism as there is no evidence of hot crust or rapid Moho depth changes.

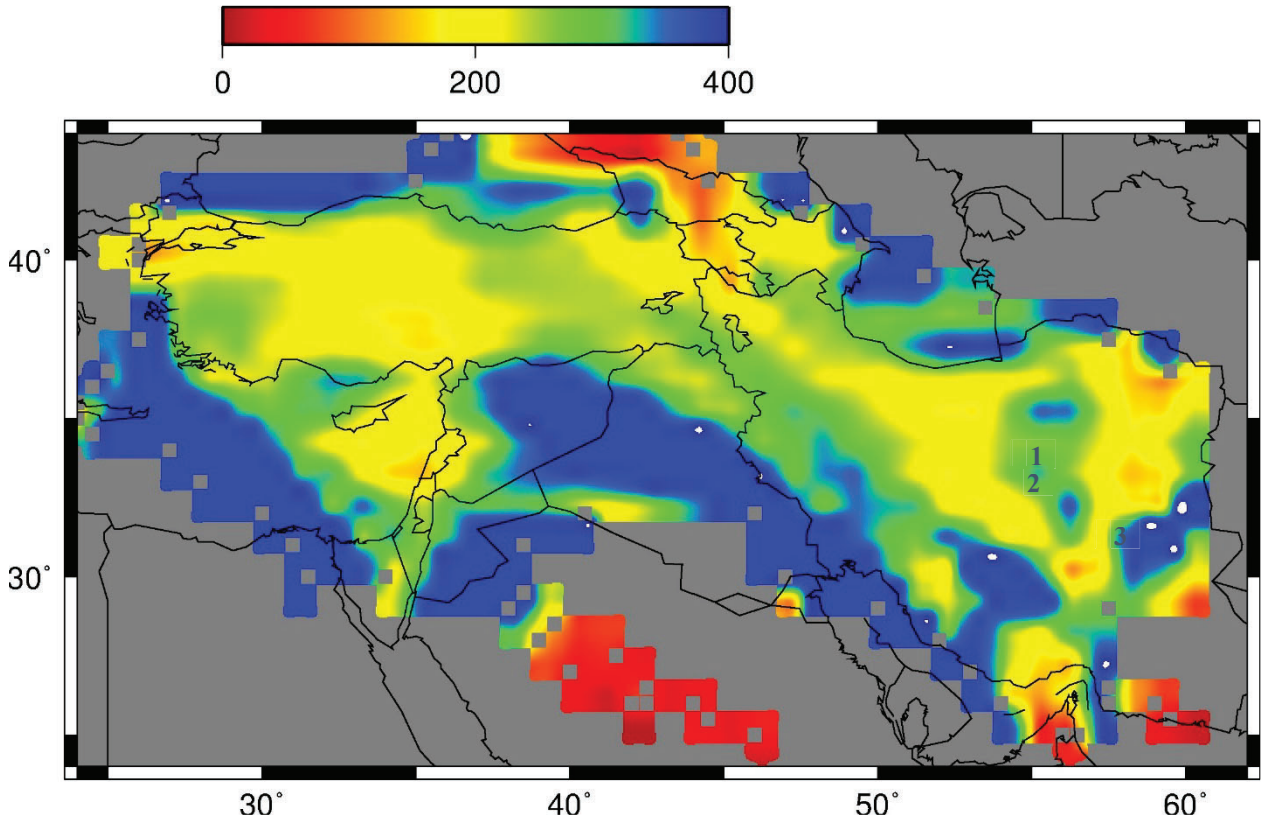

Figure 17. Caucasus Lg Q tomography at 1.0 Hz using the data from our recently deployed Caucasus Network (CNET).

We have found exceptionally low Lg Q across the western portion of the Greater Caucasus (northwestern corner of Figure 8). This very low Lg Q is consistent with the extensive blockage we have observed for paths cross the Greater Caucasus. These observations are possible because of the new seismic stations in Russia that we have acquired.

The study area is divided into 0.5° × 0.5° cells to generate tomographic models of the TSM Q at 0.5 Hz and 1.0 Hz. Only station-pair paths with efficient or inefficient Lg at the near source station are used. Figures 3 and 5 show the ray path coverage and tomographic map, respectively, for the Lg Q model at 1.0 Hz. The tomography is based on 1,141 TSM measures over 502 paths. The ray path coverage can be used to resolve lateral variation in Lg Q from eastern Armenia to central Georgia and eastern Azerbaijan. The Q values at 1.0 Hz in these areas are quite low, ranging between 50 and 150.

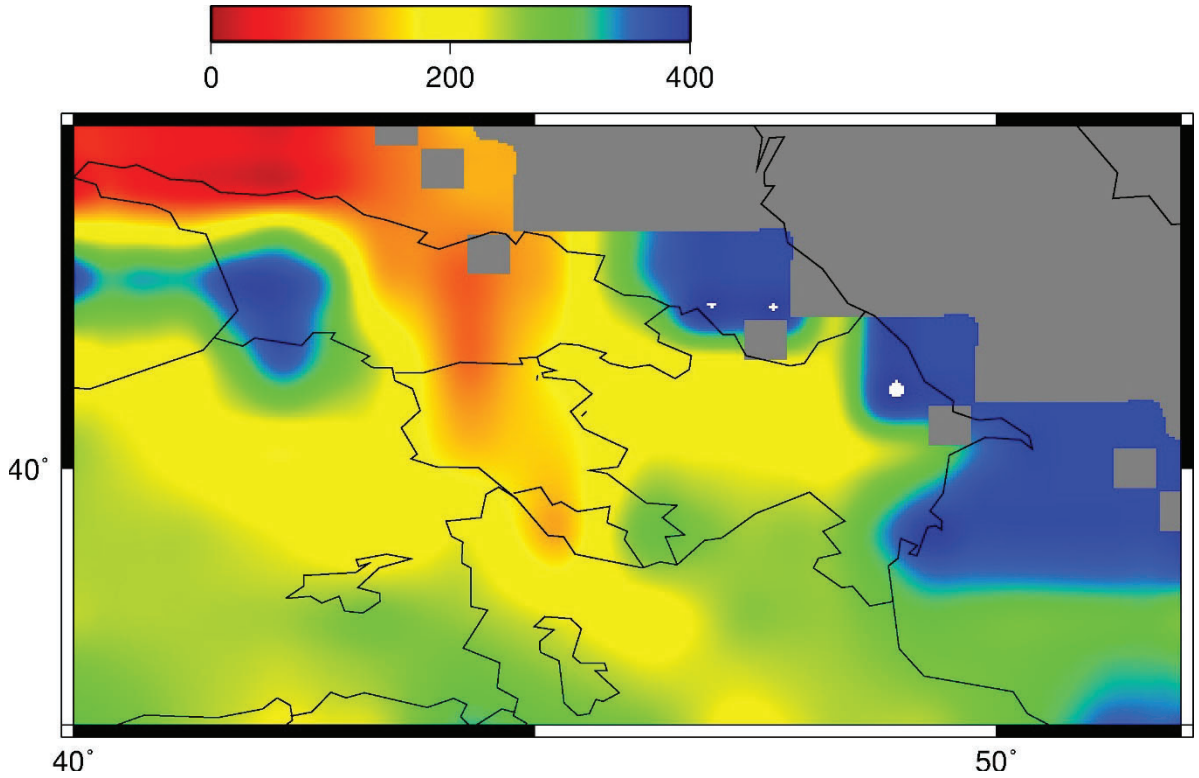

Figure 18. Map showing a zoomed-in image of the effective Lg Q values at 1 Hz across the Caucasus region. *This model is largely the result of approximately 80 new stations in the region.*

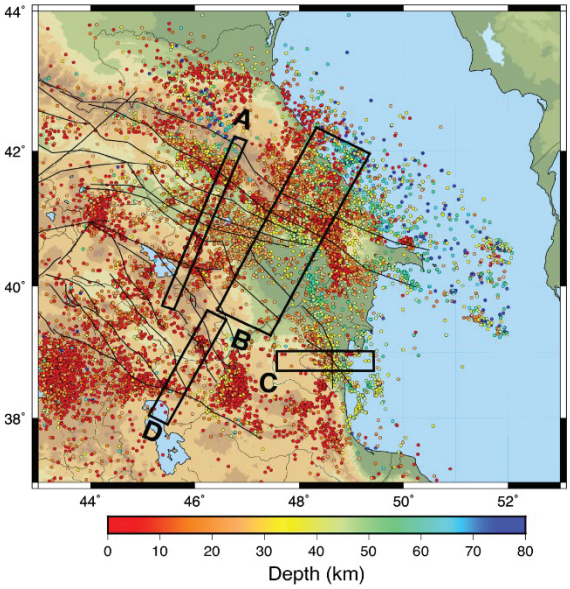

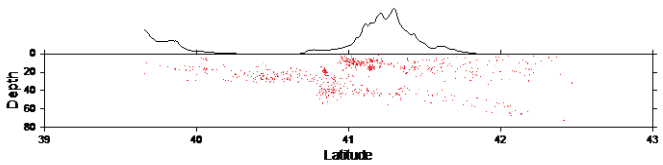

Figure 19. Epicenteral map of our earthquake relocations. *Multicolored points represent earthquake locations and the colors refer to depth. We see a large group of events in box B at 5-15 km and a separate group at 35-50 km within the Kura Basin proper. This can also be seen in the cross section of box B above.*

We have not seen a strong depth dependence of ΔQV; however, we have largely examined events in the Zagros mountains. So far, one of the key problems with using Zagros events is that the range of hypocentral depths is quite small (5-15 kilometers for

the majority of the earthquakes across nearly all of the mountain belt). Having added more RTS paths, especially in the Lesser and Greater Caucasus, we find a much larger range in hypocentral depth (Figure 19.) Figure 19 shows two very clear populations of earthquake sources that we can use to test the hypocentral depth on effective Lg Q. Furthermore, this is another region where we can test the effect of sediments and crustal root on Lg propagation. Analysis of Lg waves recorded by stations in the region suggests that the Greater Caucasus may block Lg for many paths.

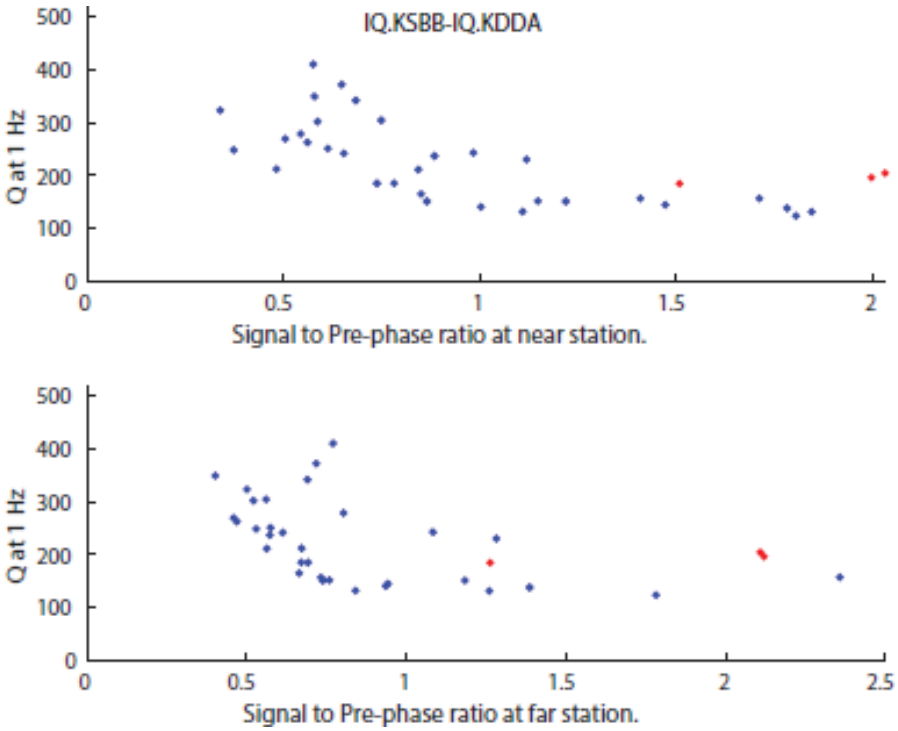

Figure 20. For a given two-station ratio (in this case a station pair contained entirely within the Iranian plateau), we plot the observed TSM Lg Q as a function of pre-phase SNR. *We observe that once we have reached a critical value in pre-phase SNR, the Lg Q values stabilize. Color indicates which side of the station pair the event lies on (red – reverse side, blue – forward side).*

4.2 Pre-Phase Signal to noise

Initially we expected this to be a relatively straightforward factor to isolate. We used both pre- event and pre-phase Signal to Noise Ratio (SNR) filters to determine the effect on observed amplitude reductions from RTS (Reverse Two Station) paths for the entire database by filtering the RTS paths with too low of SNR values. The large regional phase amplitude dataset allowed us to use stricter pre-event signal to noise ratios and still have enough repeated paths to analyze. We found that for well-resolved portions of the Sn attenuation tomography, the model did not change significantly.

We have tried to quantify the stability of the pre-phase by bootstrap resampling of our SNR model to see whether these models are stable with respect to different pre-phase

noise requirements. Our work suggests that pre-phase noise can be easily accounted for We have examined how changes in pre-phase noise for specific RTS stations pairs contribute to regional phase amplitude instability.

In Figures 20 and 21, the blue dots are pre-phase Lg SNR measurements from events coming from the forward direction (we define this arbitrarily) to the station pair and the red ones (if any exist) are those from the reversed direction. The main cause of difference between measurements from direct and reversed sides is likely to be site effect or incorrect instrument response. Our primary goal is to check the scatter in repeated measurements from each side of a station pair and understand in greater detail how pre-phase SNR varies as a function of the observed effective Lg Q. In the examples that show the Q values versus pre-phase SNR, we clearly see that the large scatter in effective Lg Q occurs is at low pre-phase SNR ratios. The low pre-phase SNR indicates that the Lg is likely to be very nearly blocked. We conclude that the main source of scatter in repeated measurements (variance in Q) is likely to be the inclusion of blocked paths. The other interesting observation we have made is that in the case of a low pre-phase SNR (likely blocked Lg phases), the Q value is systematically over-estimated. We have seen a large number of station pairs with this type of behavior.

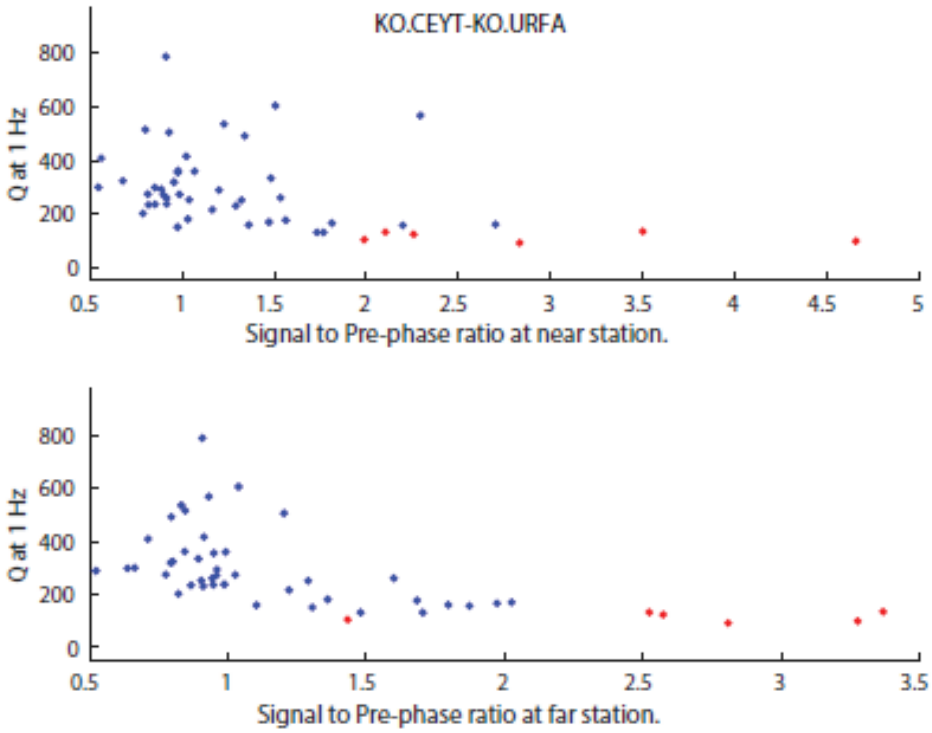

Figure 21. An RTS station pair in central Turkey using the same time analysis as shown in Figure 20. *Color coding indicates which side of the station pair the event lies on (red – reverse side, blue – forward side).*

Figures 22-25 plot LgQ versus origin date and time. Station pair IR.CHKB-IR.FIRB (Figure 22) exhibits a large variation in the measured Lg Q by event time (origin date). This is an example in which the source of Q variance is a change in the instrumentation

of stations that is not accounted for in our instrument response database. It is worth noting that we do have instrument response data that varies with time, but apparently some of these are incorrect. Station pair KO.MAZI-KO.SIRT (Figure 23) demonstrates how scatter in the measured Lg Q is not always a function of event time; in other words, we observe Lg Q to be consistent over the operation time and the source of scatter to be unrelated to any change in instrumentation.

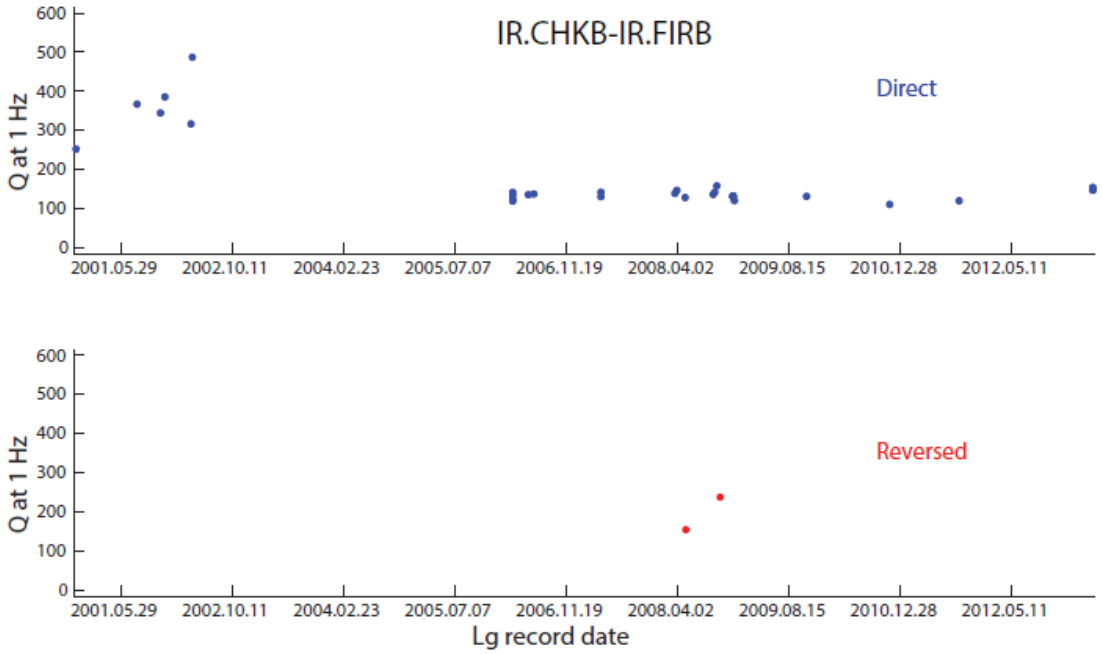

Figure 22. For a given two-station ratio (in this case, another station pair contained entirely within the Iranian plateau), the observed TSM Lg Q is plotted as a function of the TSM event date. *It appears that there is a critical date after which we see a consistent shift in the TSM Q. This would suggest an issue with the instrument response of one of these stations.*

We are have analyzed a large number of other cases of high scatter (variance) in Lg Q measurements that appear to show variation that is independent of the pre-phase SNR. The best station coverage has helped us go examine station pairs in the Iranian and eastern Anatolian plateaus, and we plan to examine station pairs in other tectonic regimes in order to test how consistent these patterns are in our data. We have developed a method to objectively map this type of behavior systematically. We have also observed a number of examples with negative Lg Q, but these negative values in TSM method are likely due to wrong instrument correction at one or both stations.

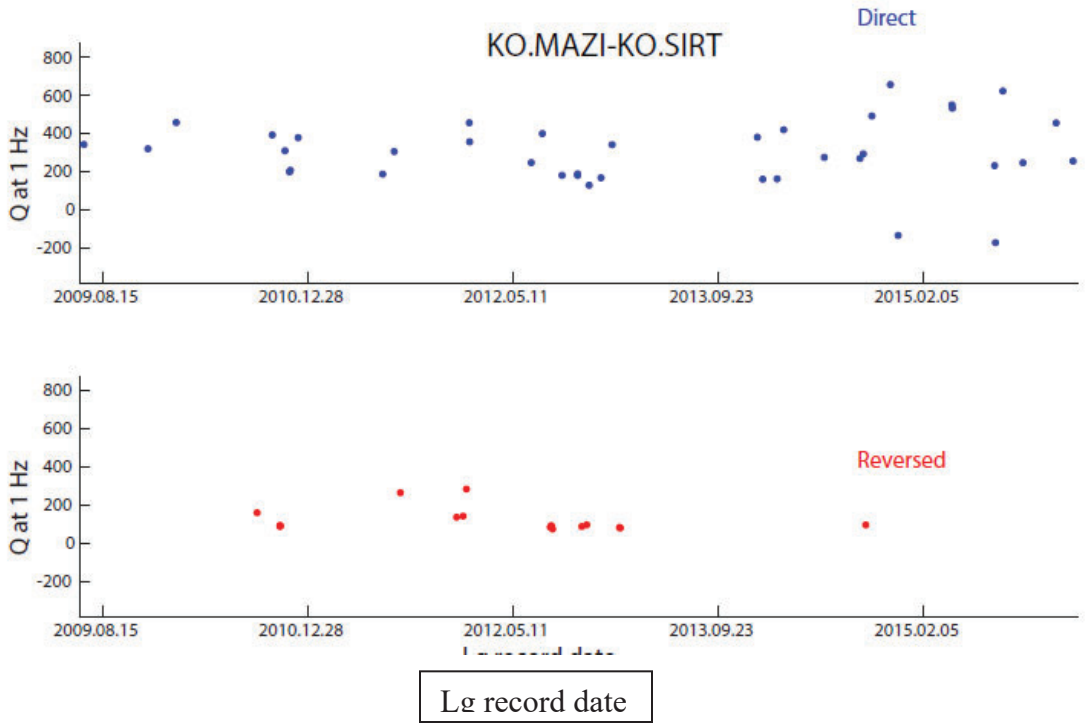

Figure 23. Another example of the same type of data analysis shown in Figure 22. *Color coding indicates which side of the station pair the event lies on (red – reverse side, blue – forward side).*

Over the course of the contract we have changed course to focus more on Two Station Method Q values as it is simpler to isolate the impact of source and station effects with this approach. This is because the contribution of the relative site response probably does not vary with time or for different sources. Therefore, this report will discuss using TSM measurements to investigate sources of high frequency amplitude instability (from the list in the introduction).

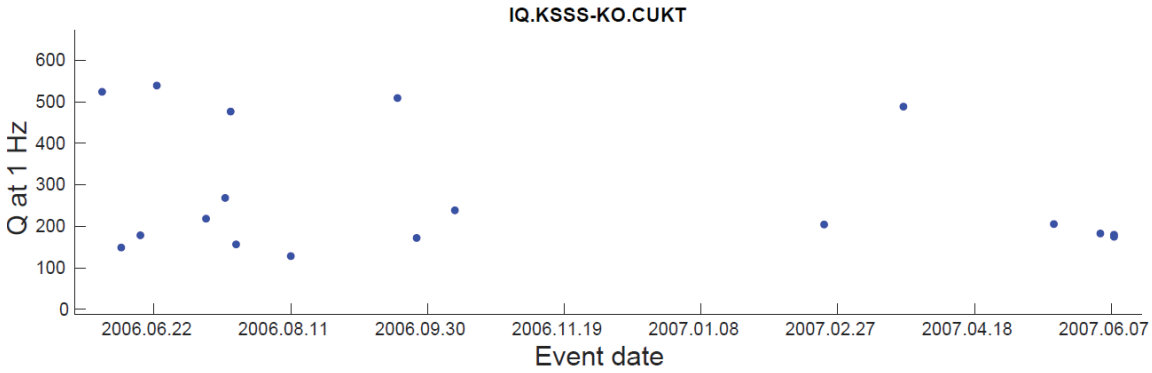

Figure 24. A plot of Two Station Method (TSM) Q values versus the origin date and time for a. two different station pairs , the top pair in eastern Turkey and the second in the Iranian plateau. *These two plots are typical of nearly all of the station pairs in our data set. These two plots are much more typical than Figure 22.*

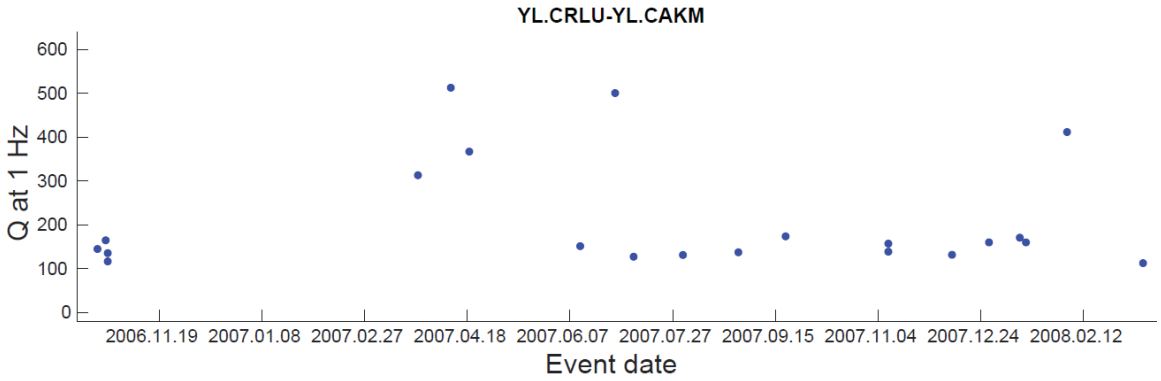

Figure 24 (continued). A plot of Two Station Method (TSM) Q values versus the origin date and time for a. two different station pairs , the top pair in eastern Turkey and the second in the Iranian plateau. *These two plots are typical of nearly all of the station pairs in our data set. These two plots are much more typical than Figure 22.*

We have identified and corrected for temporal variations in the instrument response for each of the seismic stations in our waveform database. We are particularly concerned about some of the networks that do not provide systematic metadata; however, it is worth noting that even networks with extensive meta-databases are not always correct (e.g., stations URFA and VAN in the Kandilli Observatory and Earthquake Research Institute (KOERI) network.) The Iranian network stations are the portion of our waveform database that we are most concerned about. In order to avoid the complexity of having two different source dates and times, we have changed our approach to identifying temporal variations in the instrument response by using only TSM Q measurements and analyzing how they vary with time. This approach is much more straightforward than the Reverse Two Station Method because there are two event dates in this case. Most station pairs show no evidence of this type of issue (for example Figure 24).

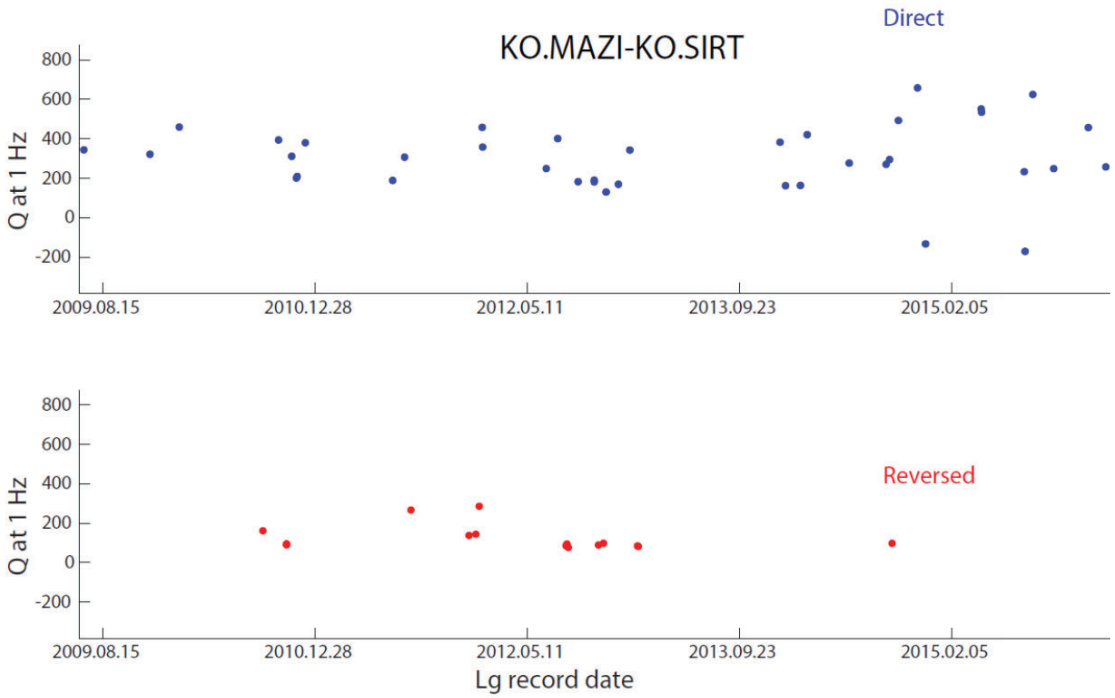

Figure 25. A plot of TSM Q values versus the origin date and time for a station pair located within the eastern Anatolian plateau. *This plot is typical of nearly all of our station pairs. We do see an increase in the standard deviation of TSM Q values after 2014, suggesting that one or both of these stations have become noisier. The two plots correspond to the two sets of events, located one on each side of the station pair (i.e., forward and reverse sources).*

We found only a few examples of clear variation in instrument response. There may be smaller temporal variations in the response but these will be harder to identify unless we have data with very large signal to noise values.

4.3 Pre-Phase SNR and TSM Q values

We have characterized the spatial dependence of the pre-phase SNR across the northern Middle East. We have tried to quantify the stability of the pre-phase by bootstrap resampling of our SNR model to see whether these models are stable with respect to different pre-phase noise requirements. So far, this approach has not shown that pre-phase noise has a significant effect. We examined how changes in pre-phase noise for specific TSM stations pairs contribute to regional phase amplitude instability.

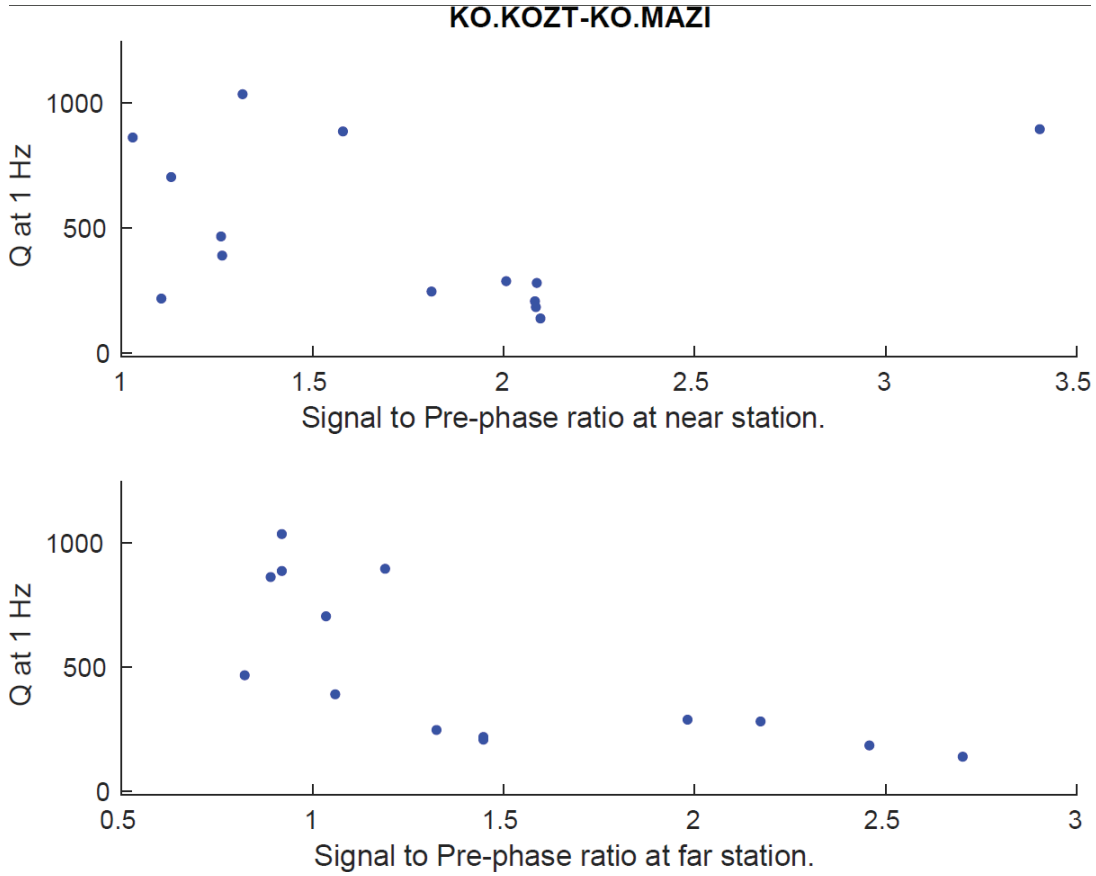

Figure 26. A plot of TSM Q versus pre-phase Signal to Noise Ratio (SNR) for a two-station pair in the central Anatolian plateau. *The two sets of plots correspond to the SNR values at the two different stations. We see with this station, as we do with most station pairs, that after pre-phase SNR values of 1.5, the TSM Q values stabilize.*

In the examples that show the Q values versus pre-phase SNR, we clearly see that the large scatter in effective Lg Q occurs at low pre-phase SNR ratios. We have finished reviewing all of the TSM station pairs and found that critical pre-phase SNR value is 1.5 for nearly all station pairs (e.g., Figure 26). There are a few cases where TSM Q values do not stabilize until pre-phase SNR values are as large as 2.0, but this is the maximum value we see before the amplitudes stabilize. Not surprisingly, there are a number of stations that never stabilize. Most of these stations are similar to the pair shown in Figure 25 in that there is no obvious temporal variation. We see clear evidence of a bimodal distribution in TSM Q values that appears completely independent of pre-phase SNR.

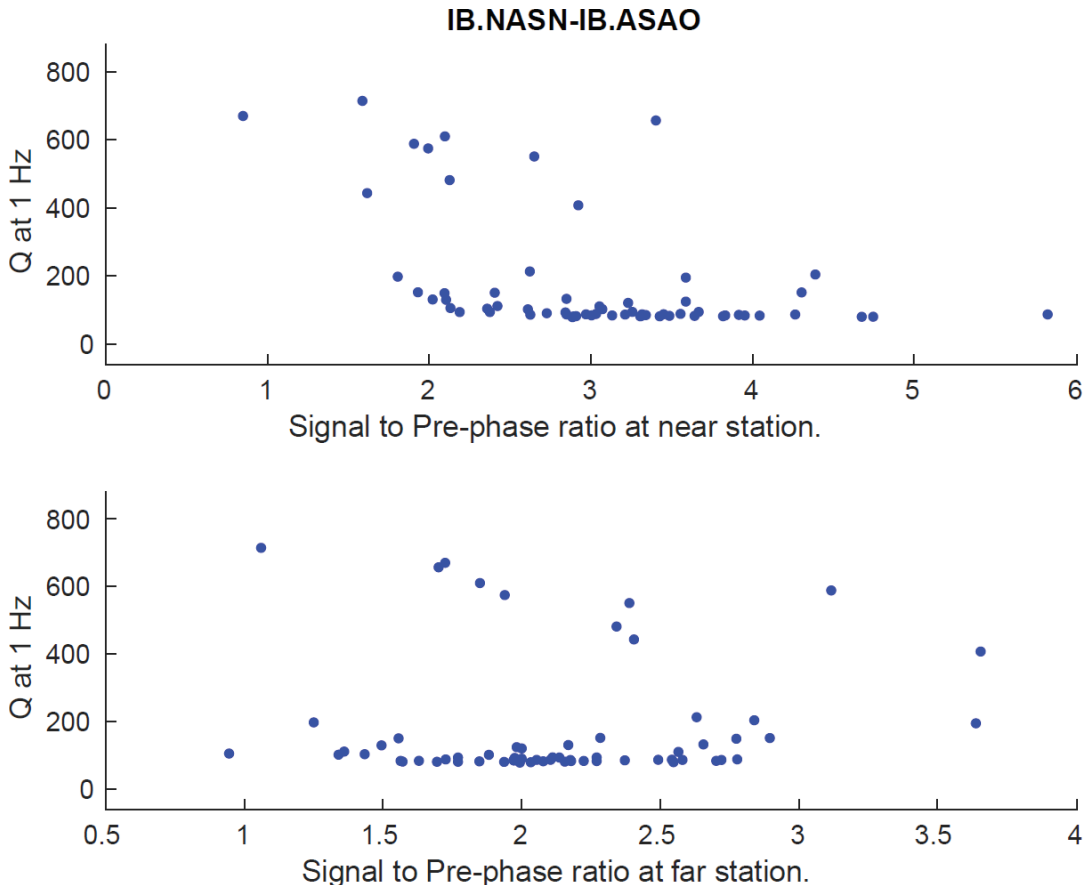

Figure 27. A plot of TSM Q versus pre-phase Signal to Noise Ratio (SNR) for a two-station pair in the Iranian plateau. *This result shows an example where despite an increase in pre-phase SNR, we still see a bimodal distribution in TSM Q values. This bimodal nature appears to be independent of SNR.*

It is clear then that not all large variances in amplitude reductions are only a function of pre-phase. Equally important is that there are serious drawbacks to setting a large minimum pre-phase SNR limit, especially in regions with small effective Q values. Elimination of small pre-phase SNR will systematically censor amplitude data sets which will effectively bias any Q model; thus, the observed stability problem is not easily solved by setting very strict pre-phase SNR values.

4.4 Depth Effect on Lg Q Instability

We have also studied the sources of the repeated Reverse Two Station (RTM) measurements of Lg Q, which effectively eliminate source and site effects. We have been able to quantify the stability and reliability of high-frequency Lg attenuation. We notice that for many regions, Lg amplitudes can be quite unstable, leading to large uncertainties in estimates of Lg $Q(f)$. We also used the Double Two Station Method (DTSM) to measure, in part, the effect of the relative change in hypocentral depth on Lg Qv. This approach has some limitations, so, we have also looked at absolute depth rather than just relative difference in depth. We have focused on relative depth because in many cases the relative depth is much better constrained than the absolute depth.

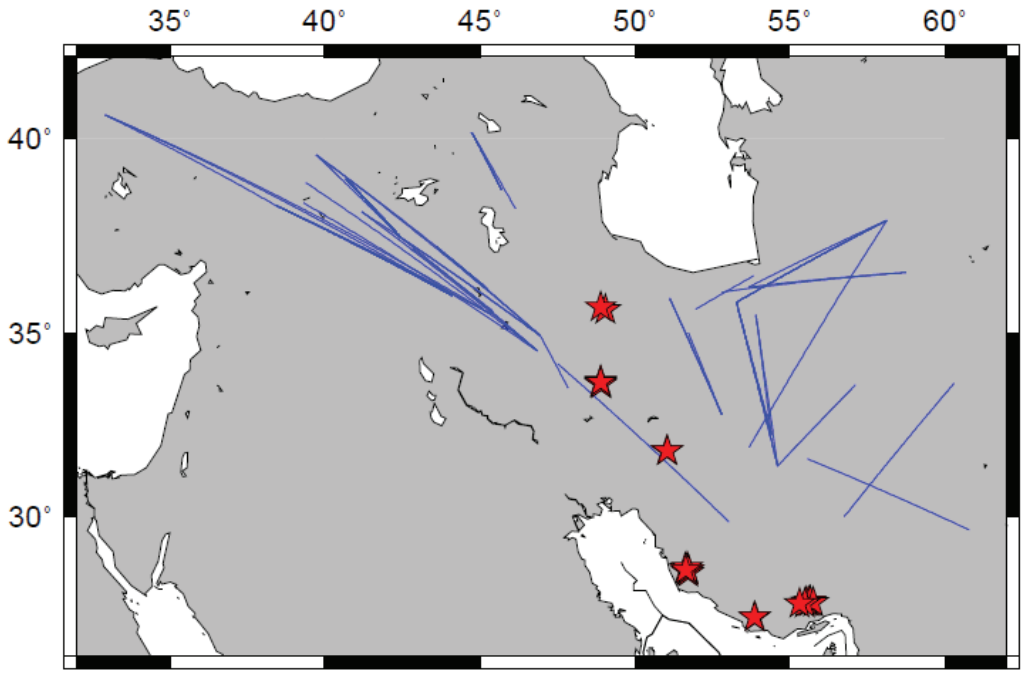

Figure 28. Event locations (stars) from the Global Catalog of Calibrated Earthquakes (GCCE) database (with all fixed depths removed) that we used to determine depth dependence and changes in Lg Qv. *The DTSM paths that we were able to extract are shown as blue lines.*

We have calculated ΔQv at 1 Hz between more and less deep events for western Iran, primarily beneath the Zagros mountain belt (Figures 8and 29). In our prior studies we have had difficulty because of large hypocentral depth uncertainties. In order to overcome this, we extracted DTSM events using the Global Catalog of Calibrated Events (https://www.sciencebase.gov/catalog/item/59fb91fde4b0531197b16ac7), where the relevant event depth errors should be less than 5 km. It is important to note that we have removed all fixed depths from the GCCE database. Interestingly we have found some evidence for consistently high Lg effective Q for greater event depths (Figure 27). This suggests that the increase in hypocentral depth would increase the Qv estimate because Lg waves from deeper events may sample a deeper part of the crust. Surprisingly, however, we observe much less change in effective Lg Q when the difference in hypocentral depths is greater than 20 km, suggesting that the greater event depths (i.e., greater than 25 km in an absolute sense) may not be reliable.

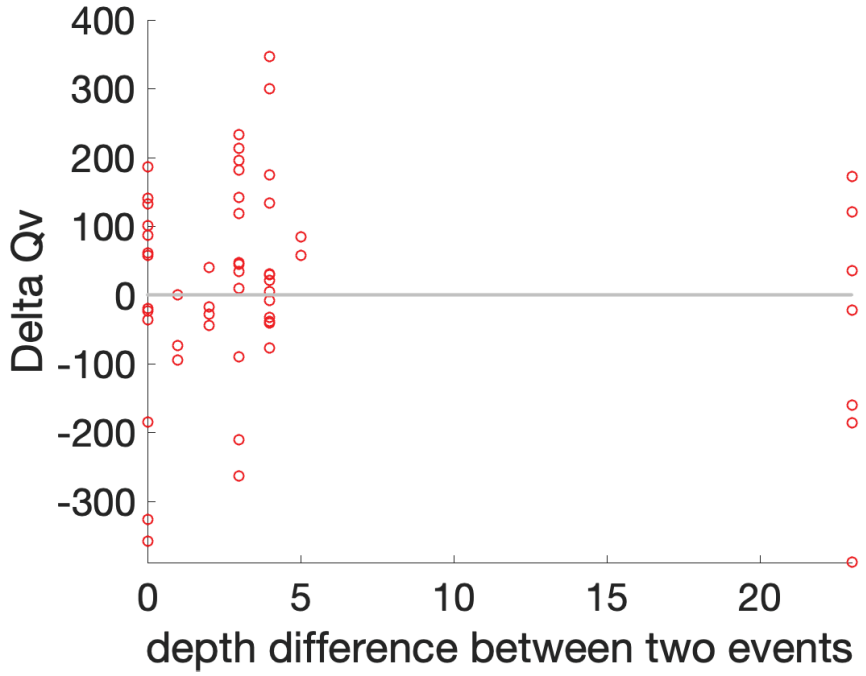

Figure 29. A plot of ΔQV for DTSM pairs from the GCCE catalog located within the Zagros fold and thrust belt as a function of differential hypocentral depth. *In this figure we use the convention* Qv_{deep} - $Qv_{shallow}$. *In other words, positive differential Qv would correspond to a deeper event, yielding a large effective Lg Q.*

4.5 Isolating Distance Effects on Effective Lg Q

We calculated ΔQv at 0.5-2 Hz between a farther event and nearer event for southwestern Anatolia, central Anatolia, and the station pair KO.SIRT_KO.BNGB, to study the effect of the source epicentral distance on the Lg Qv. It is probably advisable to repeat our definition of ΔQv. For equation 5 we have assumed that the geometrical spreading terms have become unity; in other words, we have assumed no changes in the geometrical spreading coefficient. The meaning of the subscripts in equation three depend upon the nature of the differences in source parameters being tested. The distribution in Figure 30 shows the variation in QV for a large number of different event distances. When exploring the difference in epicentral distance using equation 11, the subscripts refer to the near event (indices 1) and far event (indices 2).

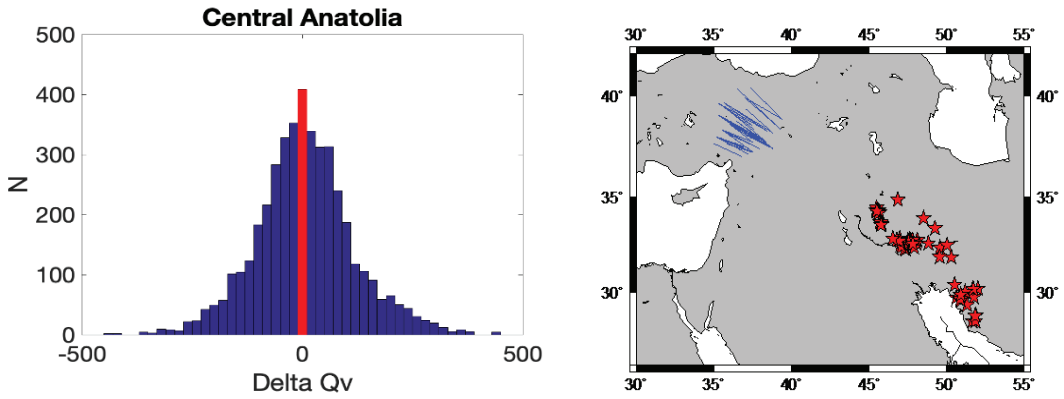

Figure 30. The ΔQV distribution at 1 Hz for Central Anatolia using TSM Q values (left). Events used (right). *This is roughly the same data set shown in Figure 28.*

We have compiled a large number of event pairs and their associated ΔQv values to look for patterns. It is necessary to have a large number of combinations in order to have a statistically significant sample size. Figure 30 shows the distribution for these results for central Anatolia and the location of the inter-station paths and event locations.

We observe a normal distribution for ΔQv values with a mean located exactly at zero. This suggests that there is no consistent variation in inter-station amplitude behavior as a function of distance. In other words, there is not a consistent difference in the effective Q for closer and farther events located in the Zagros and propagating across the Arabian plate. Given the path of these waves, generally Lg is relatively strong, but some of the more easterly events have inefficient or weak Lg amplitudes.

We have calculated ΔQv at 1 Hz between a farther event and nearer event for southwestern Anatolia, central Anatolia, and the station pair KO.SIRT_KO.BNGB to study the effect of the source epicentral distance on the Lg Qv. In southwestern Anatolia and KO.SIRT_KO.BNGB , we see a fairly clear pattern that ΔQv are mostly positive, that ΔQv increases as the distance between two events increases, and that there is a significant shift to positive values for the ΔQv distribution. For this station pair we observe that as the epicentral distance increases, so does our ΔQv estimate. This observation may be an indication that Lg waves sample a deeper part of the crust for the longer paths which leads to a ΔQv increase. For Central Anatolia, we did not see a clear pattern, however. This may be due to high levels of intrinsic attenuation caused by partial melting within the crust related to the volcanoes in central Anatolia.

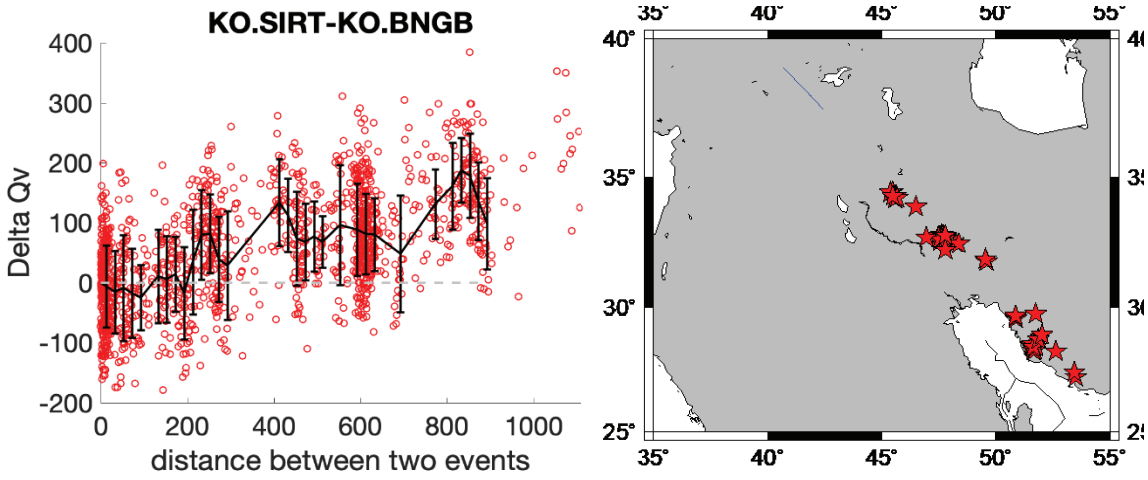

Figure 31. A plot of ΔQV for a single two-station pair as a function of the distance between the two events. *It is worth noting that this station pair is located partly in the Arabian plate and partly in the Eurasian plate (i.e., it crosses the Arabian-Eurasia plate boundary). We can see some evidence of increasing ΔQV with distance between the two events.*

An example of the two-station variation in ΔQV for a two-station path contained entirely within the western Iranian plateau just south of Iran is shown in Figure 31 and 32. The x-axis is the distance between the two locations used in the DTSM combination. We observe some distance dependence of ΔQV for distances out to 1000 km. We do not observe any structure to the distance dependence of ΔQV for events located within 50 kilometers of one another. It is somewhat surprising that even for events within 5 kilometers of one another there is no systematic reduction in ΔQV. It may be that absolute distance is more important in the behavior of ΔQV.

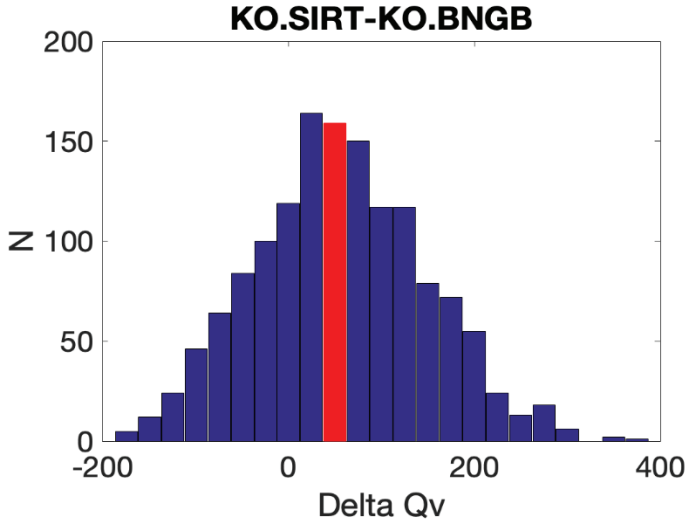

Figure 32. The ΔQv distribution at 1 Hz for the KO.SIRT-KO.BNGB station pair using TSM Q estimates. *Comparing with Figure 30, here we see a fairly clear shift in the ΔQv values that did not appear in the central Anatolia two-station values.*

4.6 Using TSM paths to Isolate Key Factors

We have learned that Two Station Method Q values allows us to much better isolate the factors that affect Q and amplitude stability the most. We have decided to take this approach because it is simpler to isolate the impact of source and stations effects. We can do this because the contribution of the relative site response likely will not vary with variations in time and for different sources. Therefore, this report will discuss using TSM measurements to investigate sources of high frequency amplitude instability. All of these seem to contribute to instability in specific regions but not across the entire Middle East.

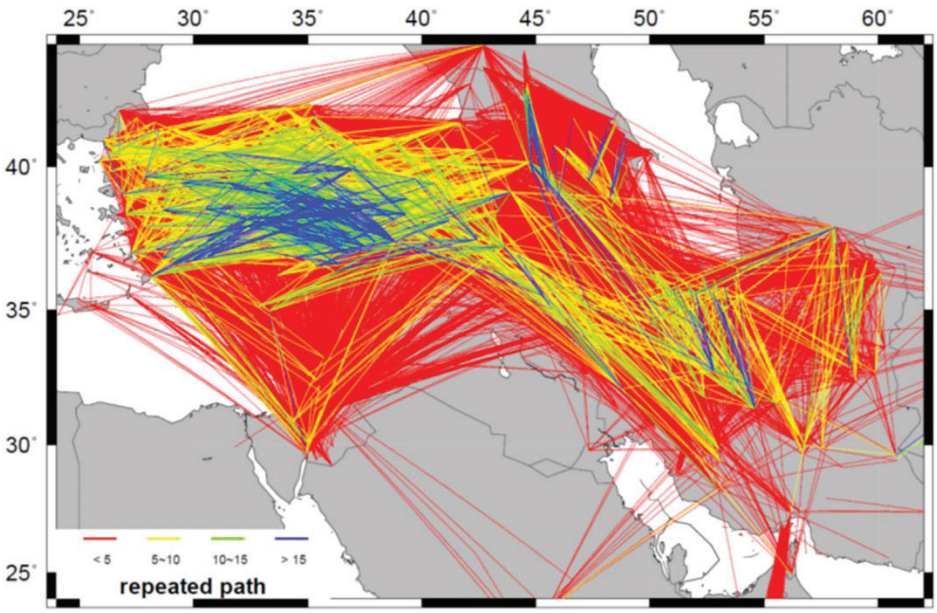

Figure 33. Reverse two station ray paths color coded by the number of repeated paths. *We have focused on those station pairs with over 15 repeated paths.*

Items 6 and 7 from the list in the Introduction have significant impact on the effective Q. In nearly all cases, however, these impacts are isolated to a given tectonic province. The lone exception may be epicentral distance, which seems to have an impact across most of the Middle East with the possible exception of eastern Turkey. In this section of our final report we present a series of plots that address these key items (on page 12) for each station pair. Figure 34 is an example for paths that run parallel to the strike of the Zagros Mountains. In the next series of figures we use Two Station Method (TSM) data to isolate temporal and spatial effects on the effective Lg Q. We have found that there are clear spatial differences in the causes in the instability of Lg amplitudes.

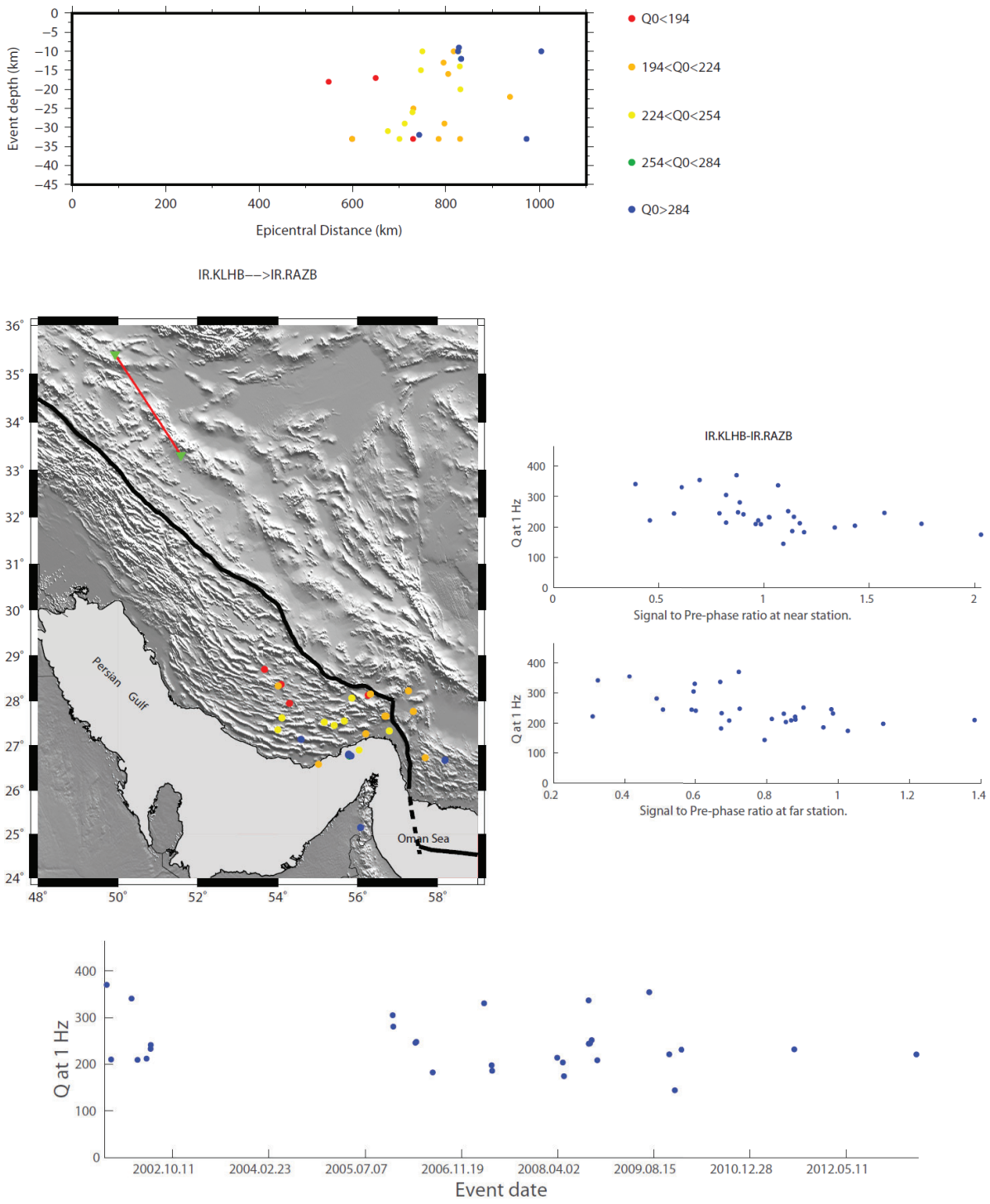

Figure 34. A combined plot showing many of the possible sources of amplitude instability for the station pair located in the western Iranian plateau. *Note that we see no temporal station dependence, but a strong distance effect on all of the effective Q measurements is shown on the map.*

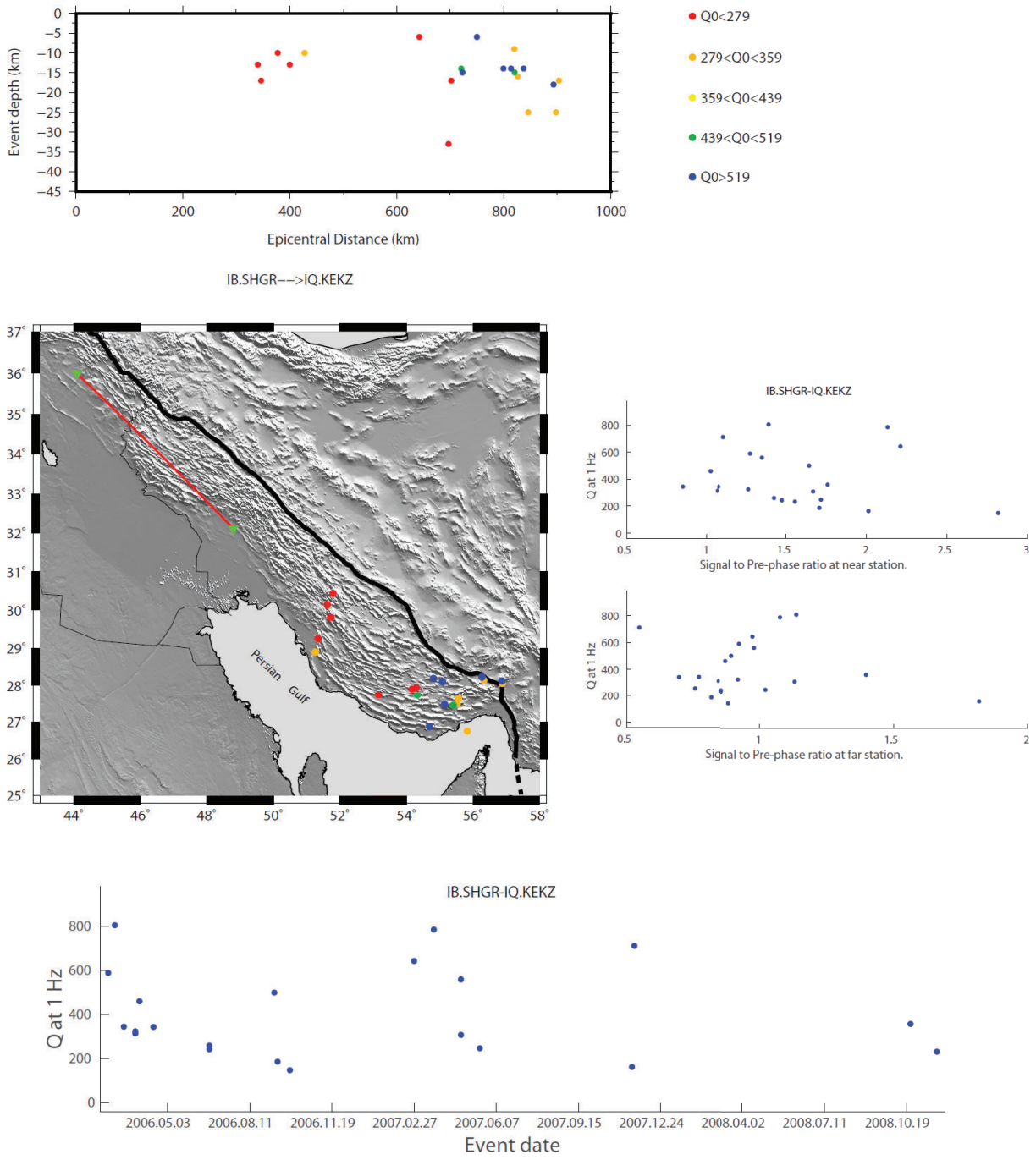

Figure 35. A combined plot showing many of the possible sources of amplitude instability for the station pair located within the northwestern corner of the Zagros Mountains in western Iran. *Note that we see no temporal station dependence but a strong distance effect on all of the effective Q measurements*.

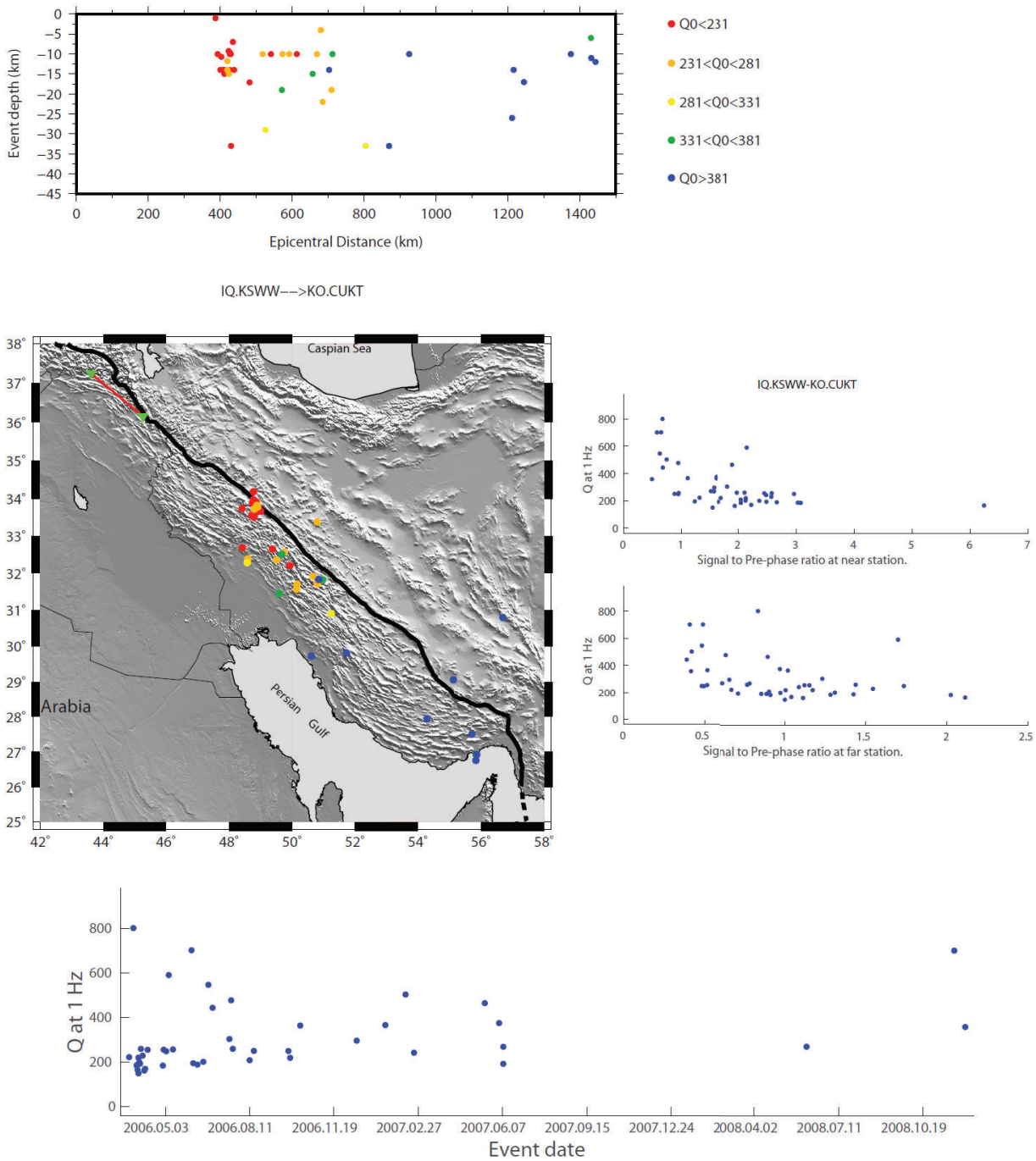

Figure 36. A series of plots similar to figure 34 for a station pair located at the northwestern edge of the Zagros fold and thrust. *Here too, we see from the map that the dominant variable on the effective TSM Q appears to be distance. We do not see depth or pre-phase SNR having any consistent influence on our estimates of attenuation.*

We have reviewed approximately 30 station pairs within the Zagros Mountains, similar to the station pairs shown in Figures 34 and 35. For most of these stations pairs the earthquakes are also restricted to the Zagros Mountains as well. First, we find that the effective Lg Q stabilizes after a pre-phase SNR of 1.0 to 1.5, which is typical for most

of the data we have looked at. With only a few exceptions do we require a better pre-phase SNR for consistent reliable estimates of Lg or Sn (see Figures 34 through 36).

We have only found a few cases of temporal changes in instrument response; once again this does not appear to be an important contributor to observed amplitude instability. As you can see in Figures 34 through 37, there is no evidence of temporal variation in the TSM effective Lg Q. This requires that there be no temporal variation significant enough to alter Lg Q estimates. Finally, we have systematically looked at distance and source effects. For the Zagros fold and thrust belt paths we see a dominant distance effect. In Figures 34 through 36 we can see a clear pattern of large distances leading to systematically large effective Q values. This is the type of variation that can explain the large variance in effective Q values that we observe even for the restrictive Reverse Two Station RTS path geometry.

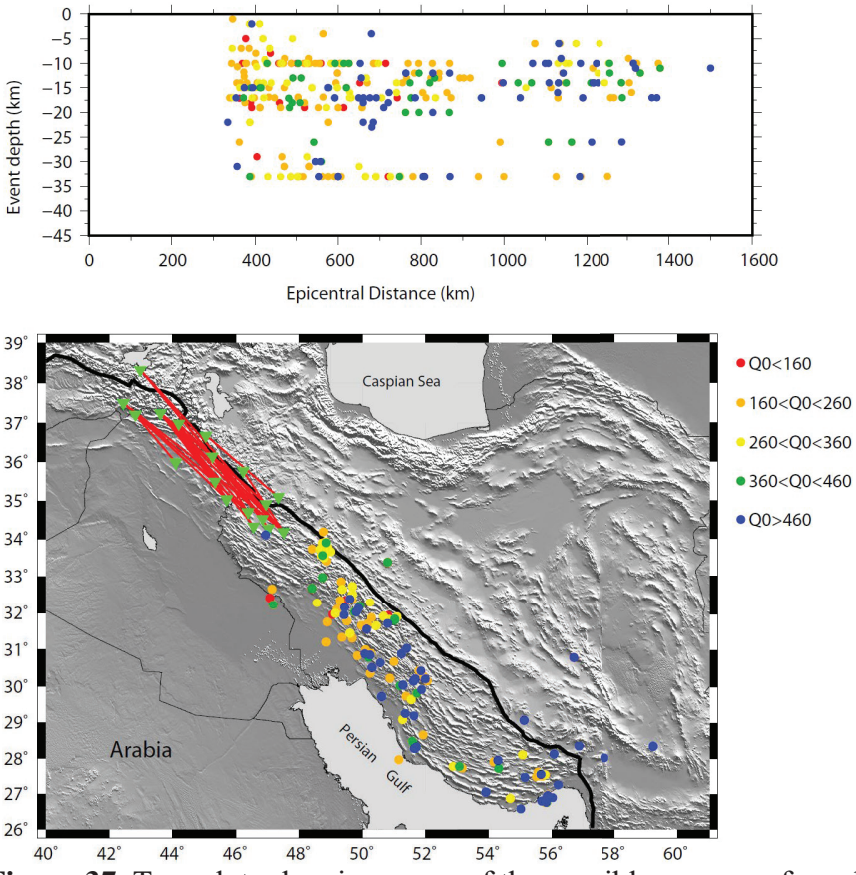

Figure 37. Two plots showing many of the possible sources of amplitude instability for station pairs located within the Zagros Mountains in western Iran. *Note that we see no consistent depth dependence but a strong distance effect on all of the effective Q measurements even when looking at a large number of station pair combinations. The variation in effective TSM Q is clearly occurring along the path and is not an effect of any station.*

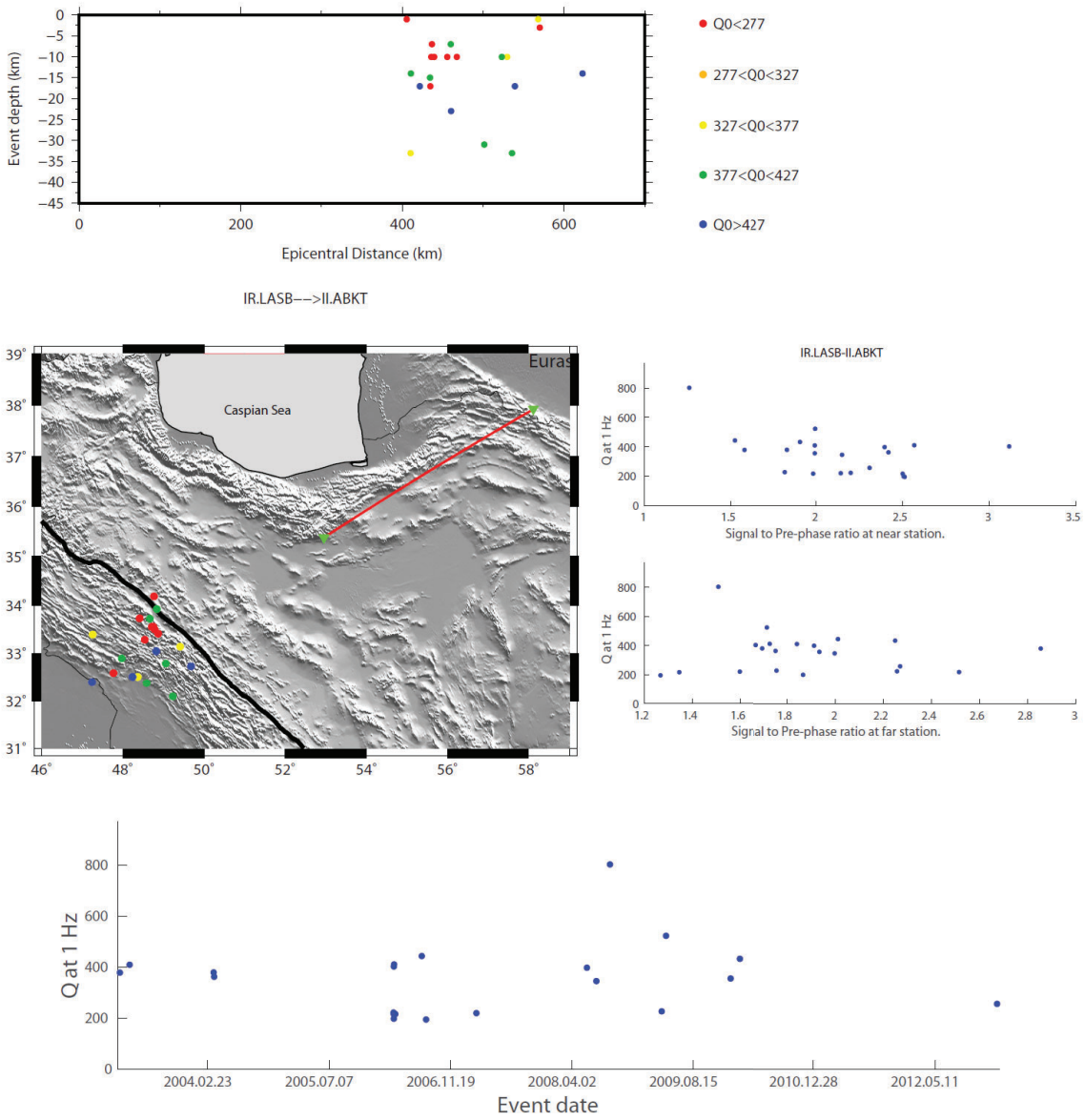

Figure 38. A plot of TSM Q values as a function of depth for the top figure; this plot may suggest some depth dependence for this particular station pair. *The middle plots show only a minor effect of pre-phase SNR rations. Finally, we also observe no consistent evidence of temporal variation in Lg Q, suggesting no significant temporal variation in instrument response. This is a typical plot for nearly all of our station pairs. Finally, on this particular path we see some consistent variation with respect to azimuth (see the map view).*

<u>Stations within the Iranian Plateau with Paths Orthogonal to the Zagros. An example of this shown in Figure 39.</u>

We have also examined two-station paths contained entirely within the Iranian plateau. Unlike our stations in the Zagros, the paths are generally oblique or orthogonal to the strike of the Zagros fold and thrust belt and the plate boundary between the Arabian and

Eurasian plates. This is likely a key difference in the factors affecting high frequency amplitude stability as well as the variance in our estimates of effective Lg Q. Again, the key factors that we have found to influence Lg Q variance are distance and source depth; however, unlike the Zagros we find that distance is not as important (although it is worth noting that we do not have as large of range of distances for these events).

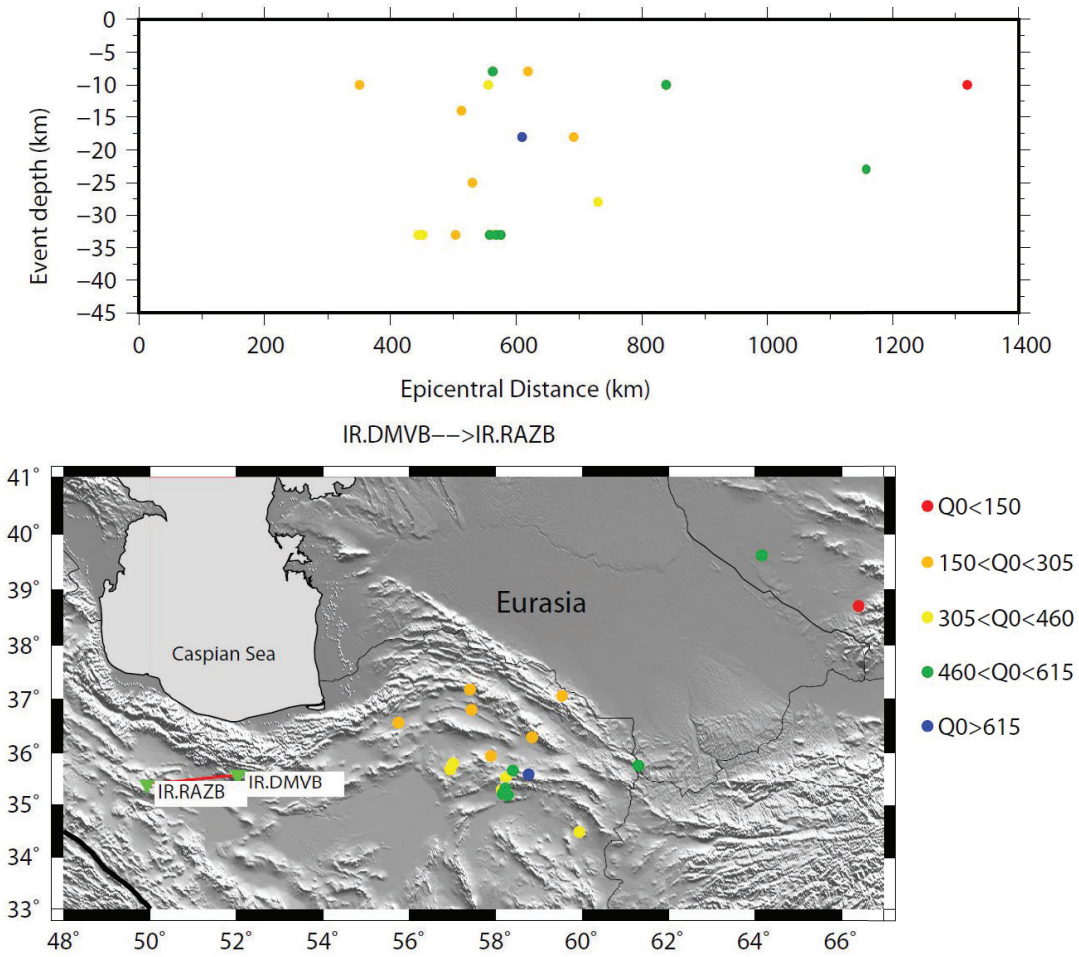

Figure 39. Plots similar to Figure 37 for a station pair located entirely within the Iranian plateau. *This is one of the unique cases where we see no clear dependence on distance, source, or source type (not shown) for the observed variation in Lg Q. It may be that source depth combined with whether the path crosses the Arabian Eurasian plate boundary can explain this variation.*

The consistent difference in behavior of TSM Q values with respect to distance between the Iranian plateau and Zagros mountain paths suggests that there is a structural difference leading to the observed distance dependence. One of the key differences between the Zagros and Iranian plateaus is the large difference in effective Sn Q values. For the Zagros paths, we suggest that there is a significant amount of Sn-to-Lg energy "leaking" into the crustal wave guide for large epicentral distances. This reduction in energy then reduces the amplitude reduction between the two stations. One could also

argue that the larger distances lead to a difference in the nature of Lg propagation between the two stations (i.e., large distances leading to Lg waves effectively traveling in large part in the lower crust). This is possible, but we would also expect to see source depth generate consistent differences in effective Lg Q values. We do not usually see this strong source depth dependence, although Figure 38 is an example where there appears to be some effect.

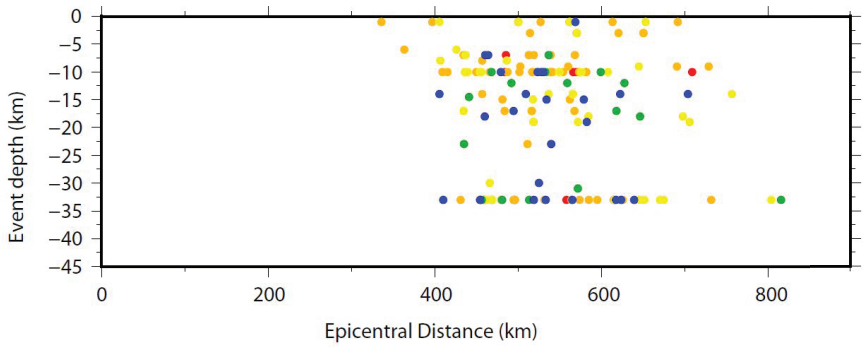

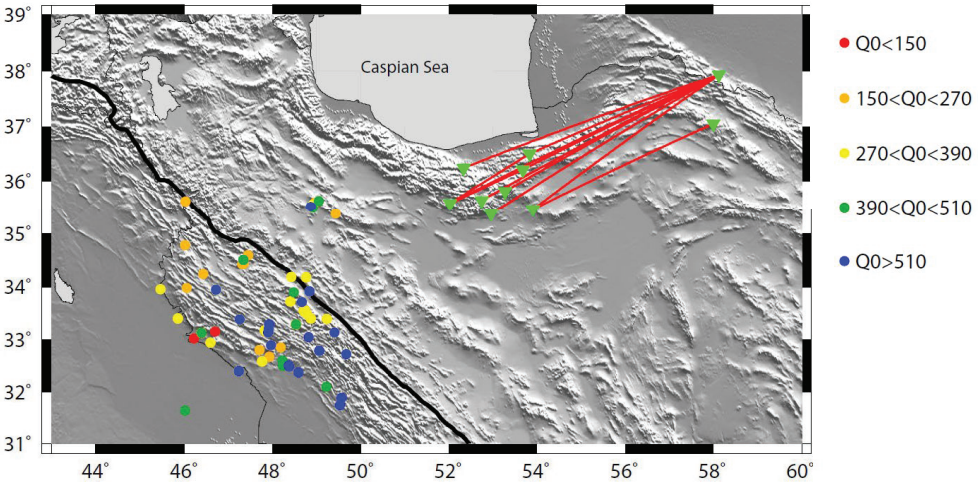

Figure 40. A collection of TSM paths for earthquakes located within the Zagros fold and thrust belt. *We can see a very sharp divide in the effective Lg Q for events to the northwest and southeast of the great circle path respectively. This kind of effect can clearly be responsible for instability in any Q estimate for Lg.*

Western Turkey

Another region where we have a large number of RTS and TSM repeated paths is western Turkey, through the use of both permanent and temporary stations. We have found that TSM effective Lg Q measurements show a strong distance dependence similar to what we have seen in the Zagros. Figure 41 is an example of this strong distance dependence. We believe this further suggests that Sn-to-Lg energy transfer is responsible for this variation. We show further examples of this type of patterns in Figures 42 through 45.

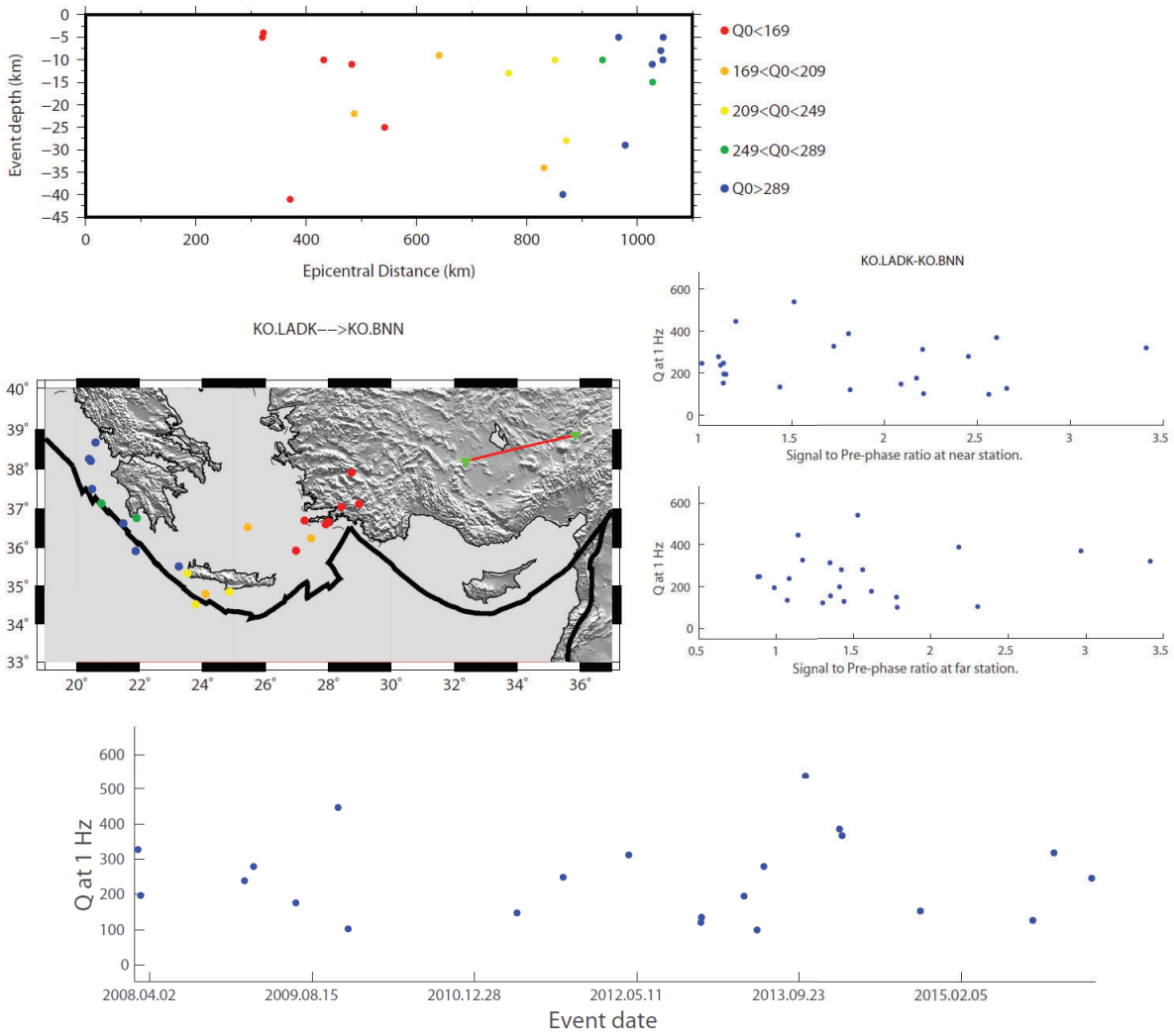

Figure 41. Another example station pair using TSM combinations for a station pair in central Turkey for events located in the Aegean and Greece. *As with nearly all cases presented in this report, pre-phase SNR and temporal variations do not appear to be responsible for the large variation in observed Lg Q values. Instead we see that distance is the key factor which is consistent with Sn-to-Lg energy.*

In summary, we find that epicentral distance is a key reason for our large variation in Lg Q estimates and suggests that most if not all Lg Q models have oversimplified how we treat the propagation of the Lg phase. Clearly, complexity in the propagation can greatly affect amplitude changes. We suggest that increasing data density should make it possible to account for these effects as secondary source terms in the attenuation models.

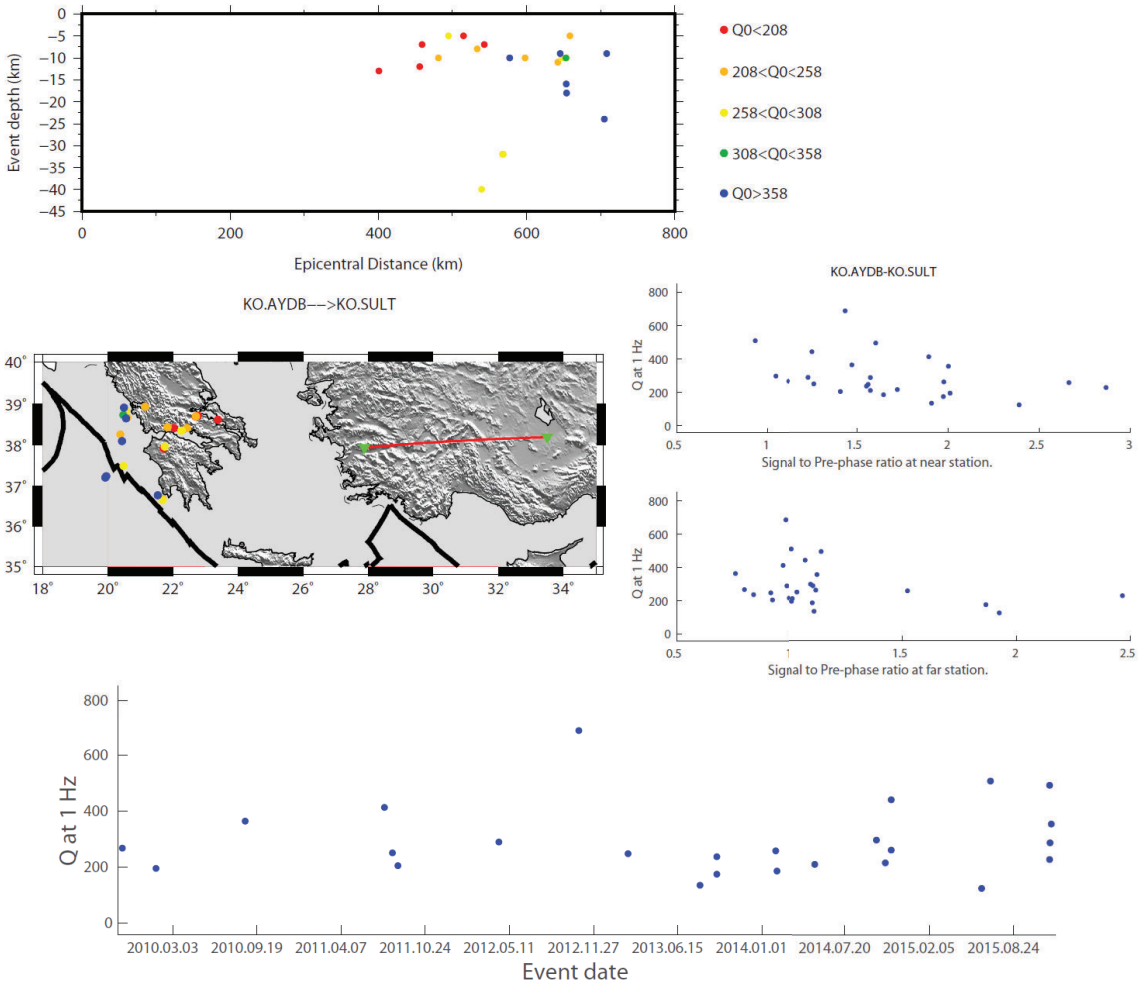

Figure 42. Another station pair using TSM combinations for a station pair in central Turkey and events located within Greece for paths that cross the Aegean Sea. *As with nearly all cases presented in this report, pre-phase SNR and temporal variations do not appear to be responsible for the large variation in observed Lg Q values. Instead we see that distance is the key factor which is consistent with Sn-to-Lg energy.*

In addition to characterizing Lg propagation from source to station, Lg efficiency can also be used to describe station-pair paths. Because blocked Lg is an indication of high crustal attenuation, comparing a blocked-path coverage map with an efficient-path coverage map can give us a basic idea about the Lg wave attenuation in the area. We see examples of the significant Lg blockage around the southeastern Greater Caucasus near the Kura thrust belt (Figure 14).

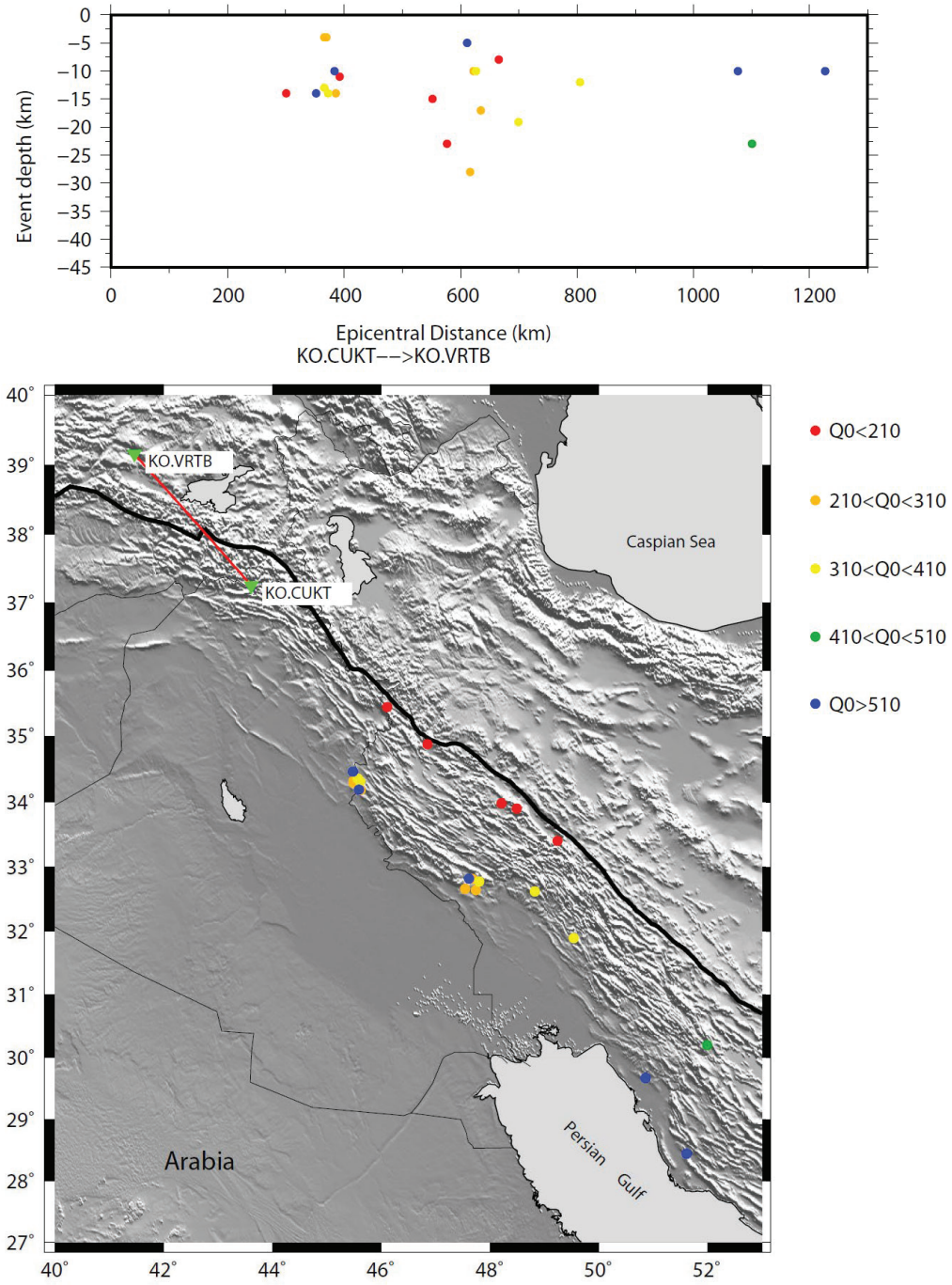

Figure 43. Another example of a station pair using TSM combinations for a station pair in southeasternmost Anatolia. *As with nearly all cases presented in this report, pre-phase SNR and temporal variations do not appear to be responsible for the large variation in observed Lg Q values. Instead we see distance as the key factor, which is consistent with Sn-to-Lg energy.*

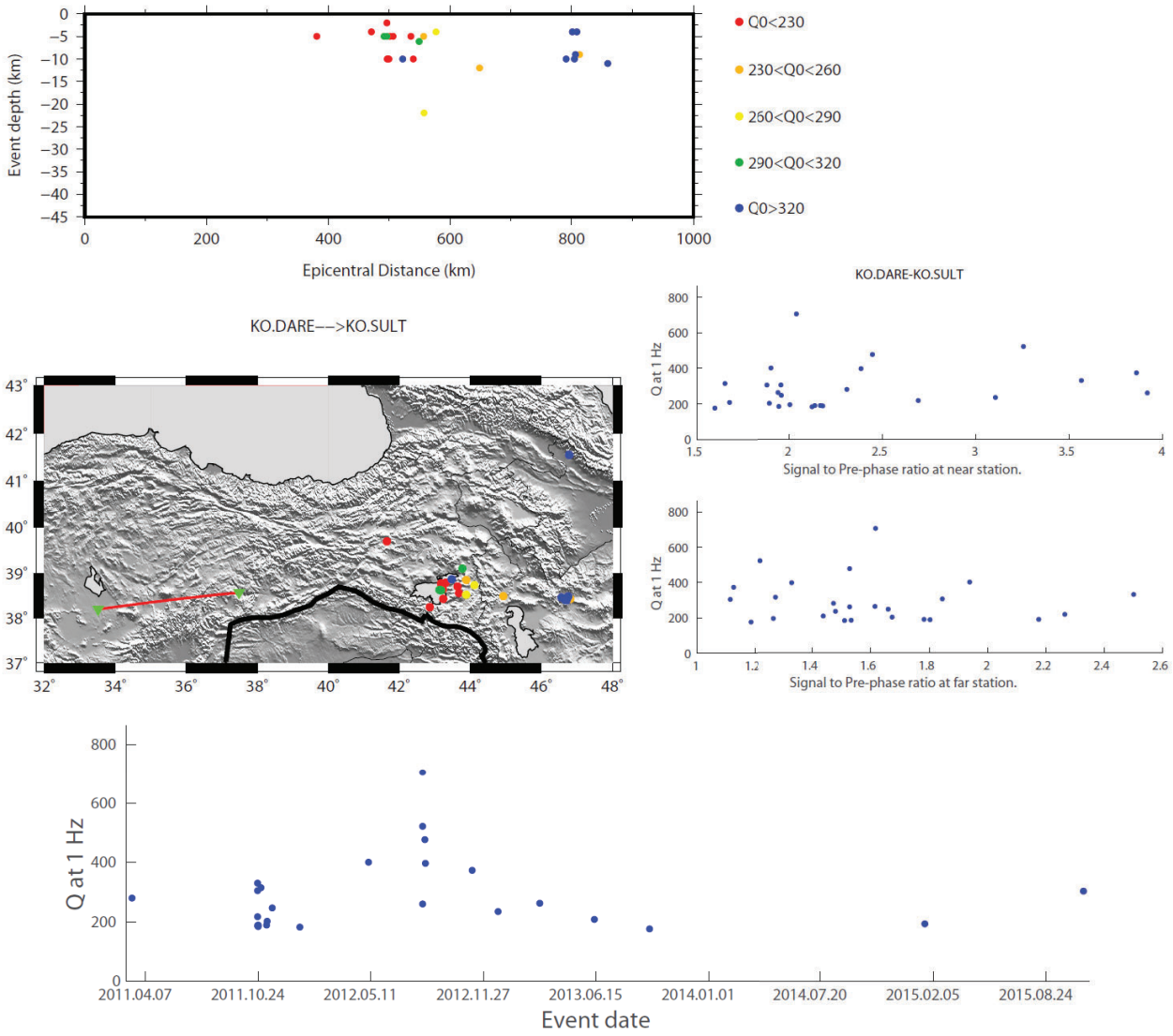

Figure 44. Another key station pair using TSM combinations for a station pair in central Turkey. *As with nearly all cases presented in this report, pre-phase SNR and temporal variations do not appear to be responsible for the large variation in observed Lg Q values. Instead we see that distance is the key factor, which is consistent with Sn-to-Lg energy*.

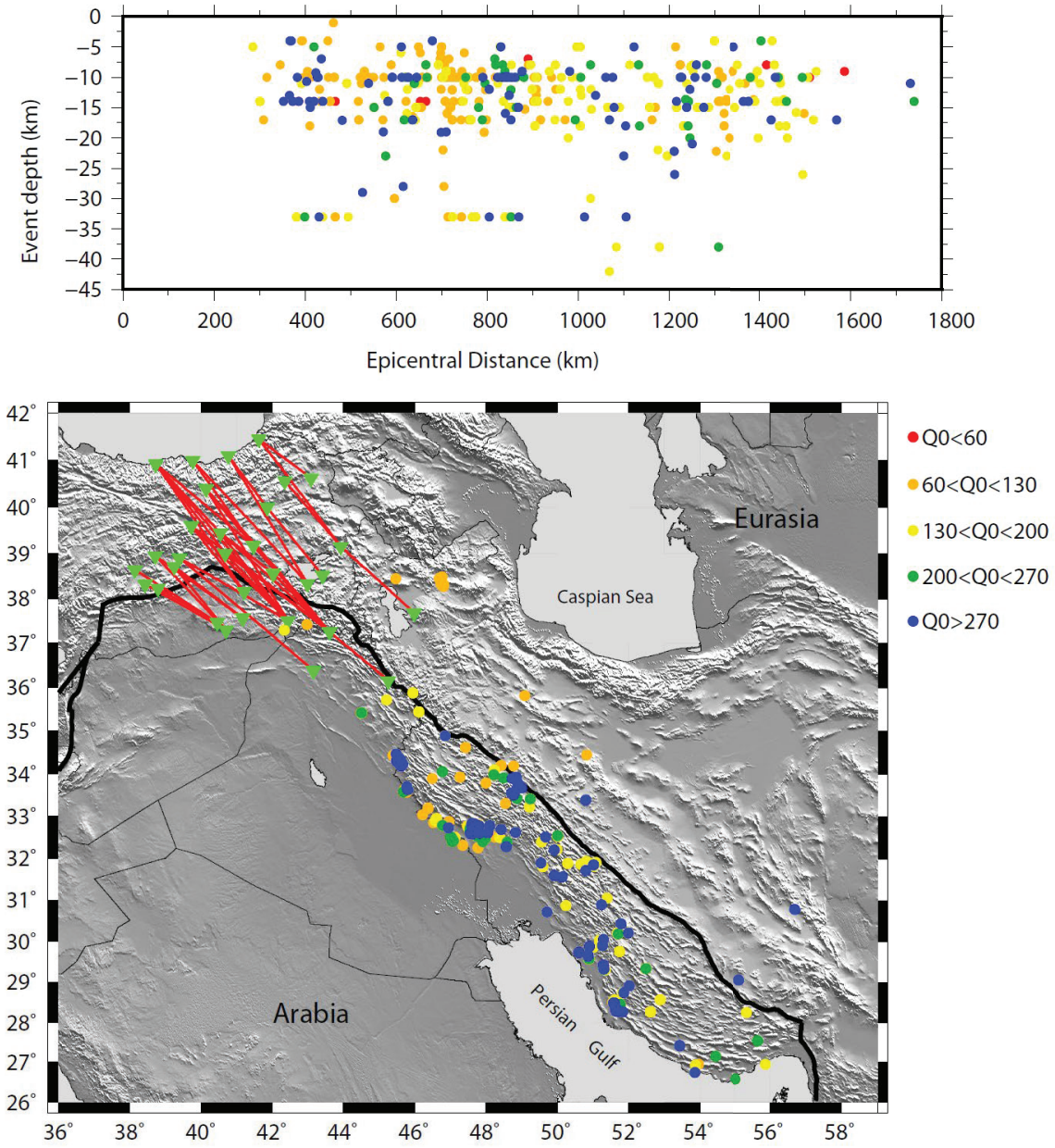

Figure 45. Another key station pair using TSM combinations for a station pair in central Turkey. *As with nearly all cases presented in this report, pre-phase SNR and temporal variations do not appear to be responsible for the large variation in observed Lg Q values. Instead we see that distance is the key factor, which is consistent with Sn-to-Lg energy.*

4.7 Impact of Focal Mechanism on Lg Q Instability

One of the explanations for some of the observed Lg Q instabilities is that the focal mechanism, or more specifically, the three-dimensional source radiation pattern, can lead to systematic variations in Lg Q with respect to absolute azimuthal variation. In this scenario, different radiation patterns may excite different modes of Lg propagation between two given stations for example for Lg paths on either side of the great circle

path. It is possible that if Lg waves propagate differently for a given direction with respect to a given focal sphere, we may observe a systematic difference in TSM Lg effective Q. Perhaps SNR might also bias the observed effective Lg Q. This would mean that if for a given portion of the source radiation pattern Lg is weaker, it could have some impact on the Lg SNR and thus possibly bias the observed Lg Q.

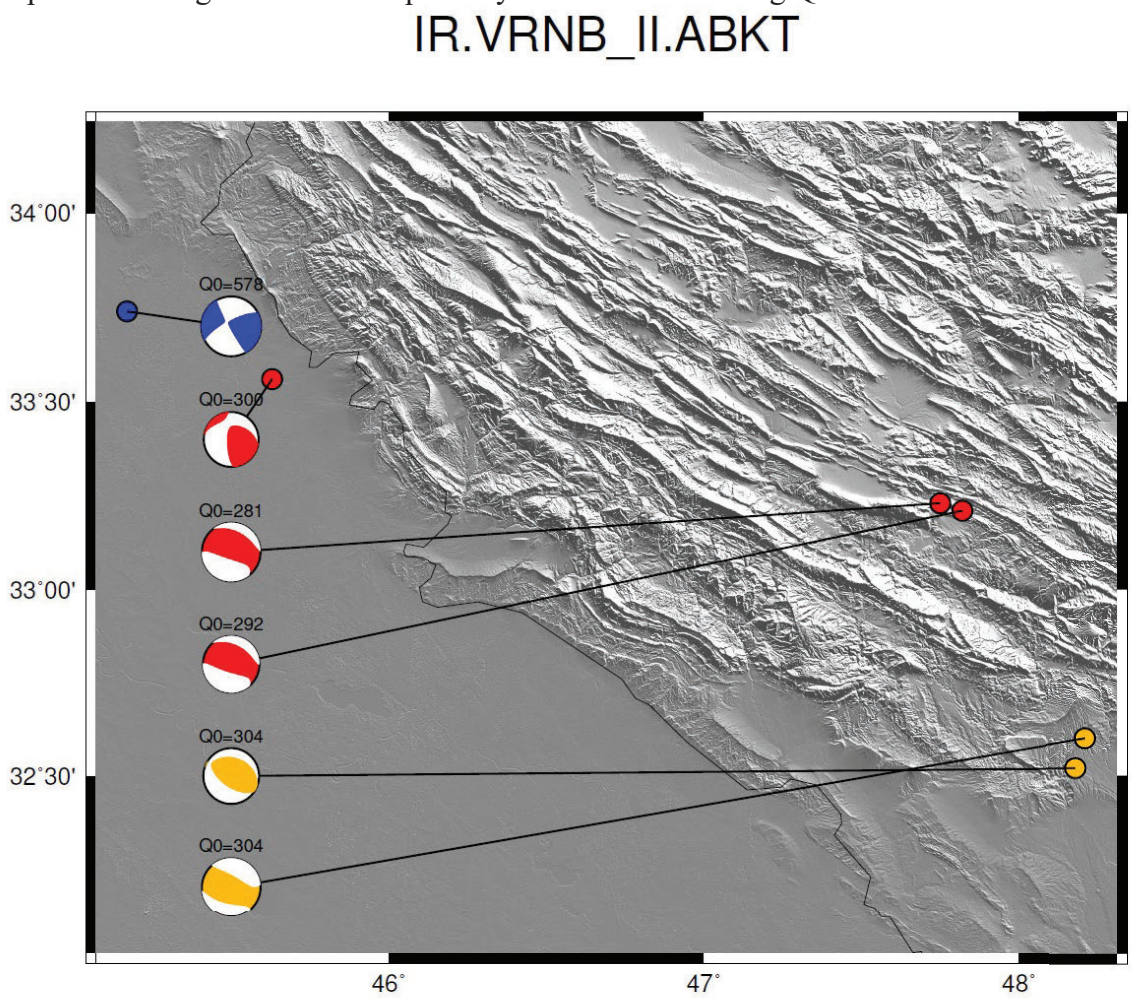

Figure 46. Six different focal mechanisms for six events used for TSM Q estimates for the station pair VRNB and ABKT. *This path extends across the northeastern part of the Iranian plateau. The focal mechanisms are color coded by the TSM Lg Q values (hotter color correspond to lower Lg Q and colder colors to higher Lg Q) that we have calculated between this specific station pair.*

In order to test the idea that different focal mechanisms lead to differences in observed TSM effective Lg Q values, we have collected a large number of focal mechanisms for the set of events where we observe systematic differences in effective Lg Q as a function of azimuth (see for example the map in Figure 40). We have plotted the focal mechanisms for all of the individual paths for all TSM station pairs to determine whether there is a strong correlation between the focal mechanisms and the Lg effective Q (Figures 46 and 47). In general, we observe no correlation between focal mechanisms and effective Lg Q value.

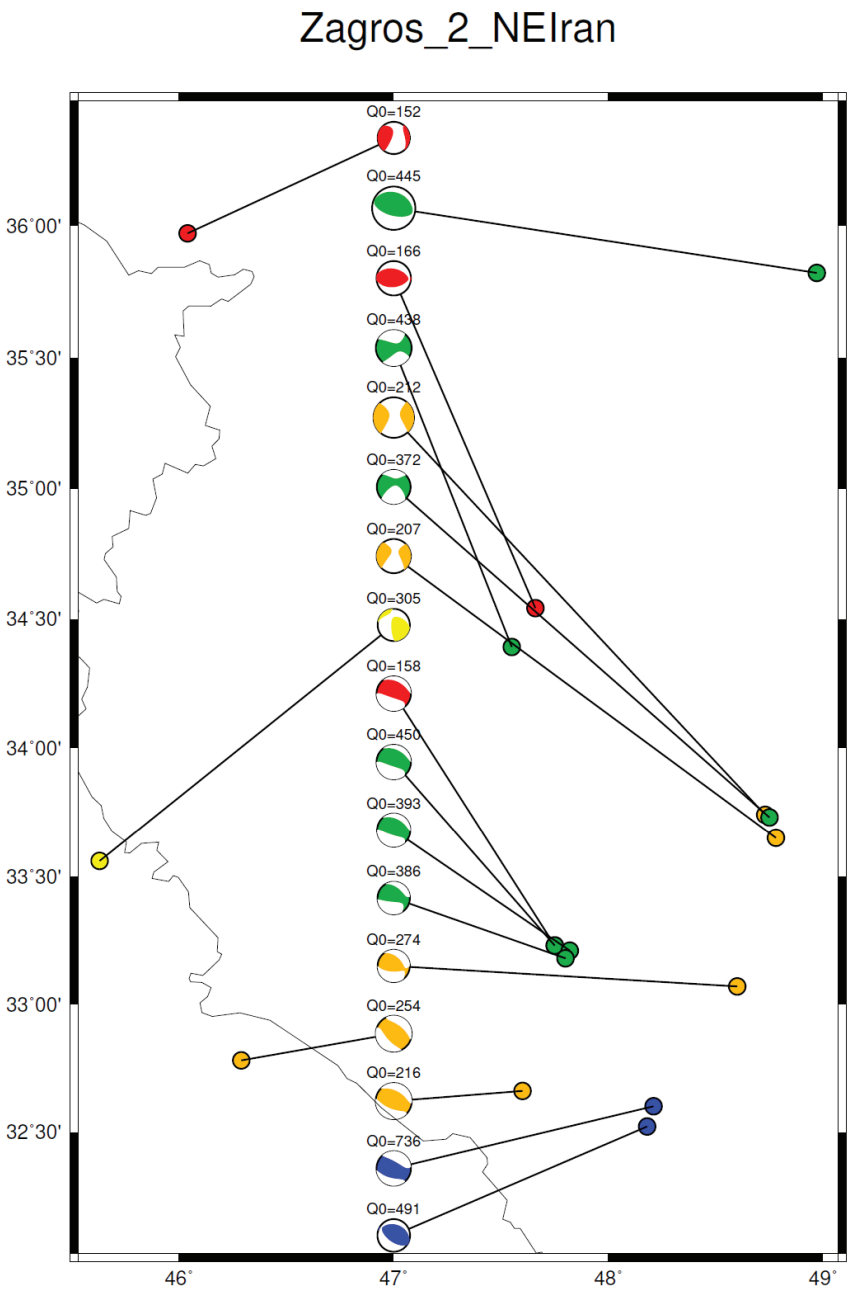

Figure 47. Focal mechanism plot for all of the events shown in Figure 40 that have a focal mechanism in the Global Centroid Moment Tensor (GCMT) catalog. *Similar to Figure 46, we have color coded the focal mechanism by the average effective Lg Q for all of the TSM pairs shown in Figure 40. Hotter colors correspond to lower observed Lg Q at 1 Hz.*

In order to convey the totality of our findings and not just focus on individual paths, we have summarized our comparison of effective Lg Q and the corresponding focal mechanism in Figure 40 where observe systematic variations for different source locations within the fold and thrust. Examining our result, we see that there is a mixture

of strike slip and thrust focal mechanisms. We do not see a clear separation in Lg Q value and strike slip and thrust mechanism. Furthermore, it does not appear that the strike of the fault has a significant impact on Lg Q.

4.8 Estimating Source Terms

We have worked to estimate source terms for several events located within the Iranian plateau given to us by AFRL. We have assumed the following formulation:

$$S(f) = \frac{A(f,\Delta)}{A^*(f,\Delta)} \tag{13}$$

where

$$A^*(f,\Delta) = G(\Delta)R(f)e^{\frac{-\pi f \Delta}{Qv}}$$

G is the geometrical spreading function, R is the site response, A is the frequency dependent observed Lg amplitude, S is the source term, and A* is the model-based amplitude based upon only the path and site components of equation 1. We assumed a constant geometrical spreading function of Δ^{-1} for the entire model because this is what was assumed when calculating the Lg Q(f) and R(f) models (the range of results are shown in Figure 48).

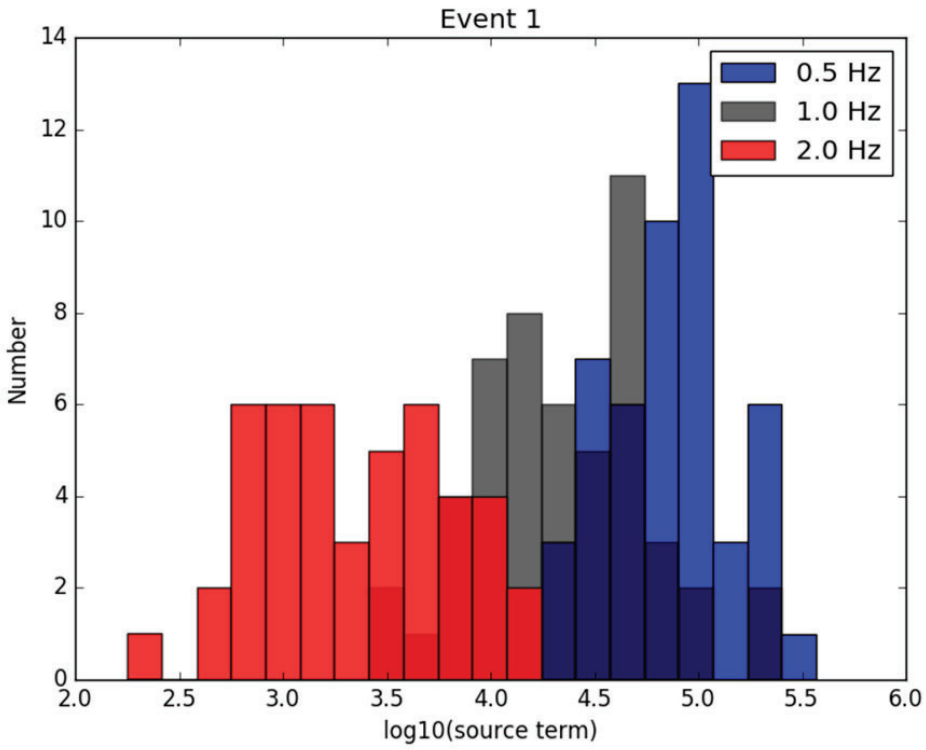

Figure 48. The estimated source terms for all available stations using our Lg Q model. *The colors are coded by frequency for one of our test events.*

Using equation 12, our published frequency dependent Q, and our new site response model, we have estimated the source terms using approximately 50 stations for the largest Iranian plateau event of the three events that had independent source parameter estimates. We observe, as we would expect, that the source term decreases with increasing frequency. We have seen that the instability or standard deviation of the source terms also increases with increasing frequency. Figure 49 shows the source terms as a function of frequency for the largest of the three events.

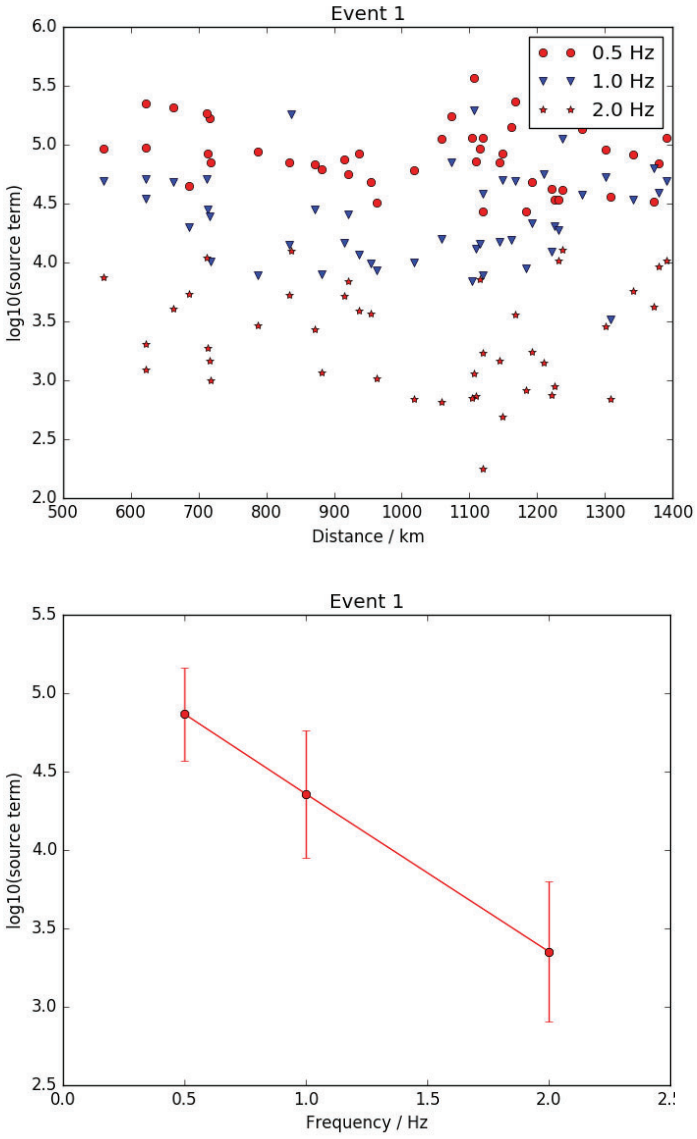

Figure 49. A plot of the Lg source terms derived from our waveform database for a Mw 5.3 earthquake recorded by stations mostly in the Iranian plateau. *In the lower panel we can see the standard spectral decay for the terms as a function of frequency.*

4.9 Stability of Regional Phase Coda

In addition to studying direct phase amplitudes, we working to measure the inherent uncertainty in coda across the Iranian and Turkish plateaus. We are using all of the same data from our work on the Lg phase to measure different aspects of coda in order to construct a model for how coda parameters vary in two dimensions across the northern Middle East. This work is allowing us to compare Q values obtained from source corrected amplitude spectra. In order to better characterize source characteristics to improve attenuation models, we used the empirical technique of Mayeda et al., 2003 and Gok et al., 2016, to measure coda parameters for the Iranian plateau. An example analysis is shown in Figure 50. We mapped variations in these parameters as a function of distance and 14 narrow frequency bands (0.03-8 .0 Hz). We are investigating these differences by utilizing a detection framework technique to form the correlations of envelopes and identify how they would cluster and form similarities as a function of depth, regional phase and tectonic feature. We already observe substantial differences in regional calibrations of coda envelopes at high frequencies throughout various tectonic regimes. One of the dominant factors influencing coda parameters is whether the main S-wave arrival is Lg (for continental paths) or Sn (for oceanic paths).

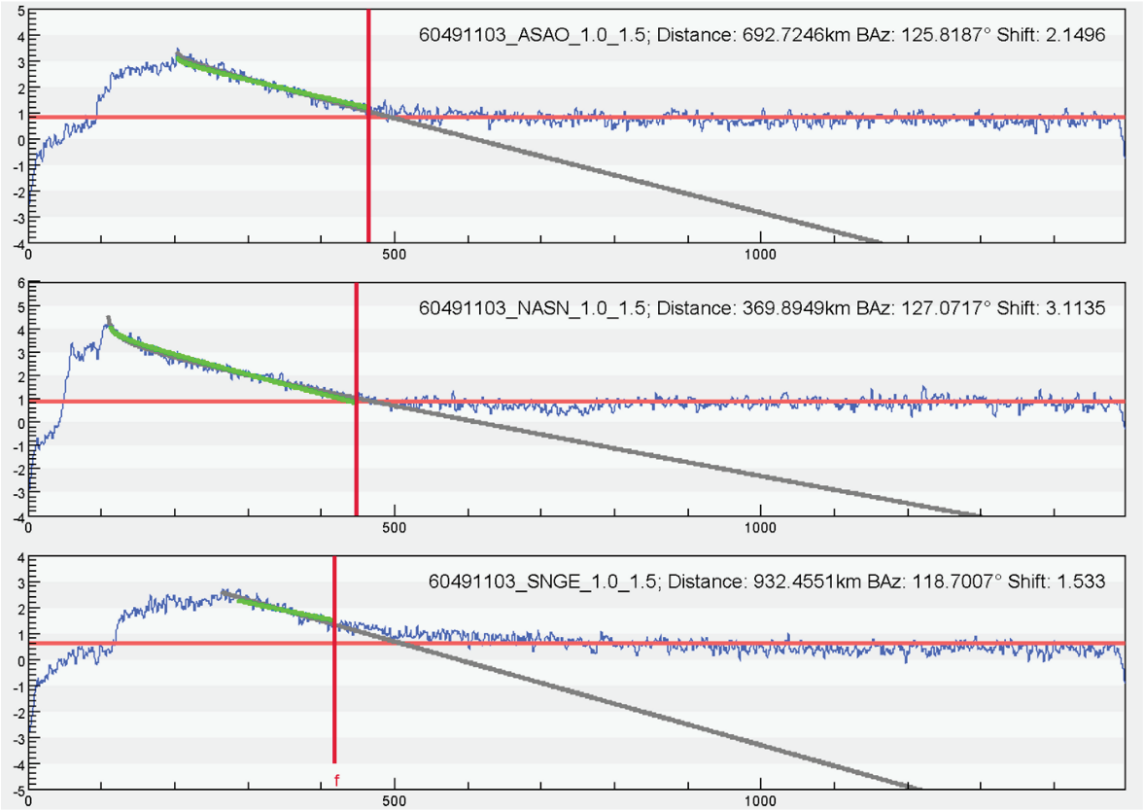

Figure 50. An example of coda envelopes for three stations within the Iranian plateau. *The red line is the termination of the coda window and the green line is the best fit of the coda envelope for each waveform.*

We have worked to calculate coda envelopes using the method laid out by Gok et al., 2016 and the same database that we used to study direct amplitude stability. This work

utilizes the spectra of background noise and that of the desired window of the phase under consideration (Lg, Pg or Sn). The position in time of the coda envelope can be used to calculate the coda window velocity (Figure 51). We can see there are systematic variations in coda velocity across the Middle East. This is primarily a function of whether the paths are principally oceanic or continental. For continental paths the largest amplitude is typically Lg and thus the coda velocity corresponds to the end of the Lg group velocity window. For oceanic paths, seismograms are dominated by the Sn and Pn phases; thus the coda envelope velocities are consistent with Sn velocities. One can observe these oceanic paths when looking at Figure 51; however, we observe a relatively strong frequency dependence to this effect suggesting that the Sn signals typically consist of higher frequency amplitudes when examining the coda envelope velocities.

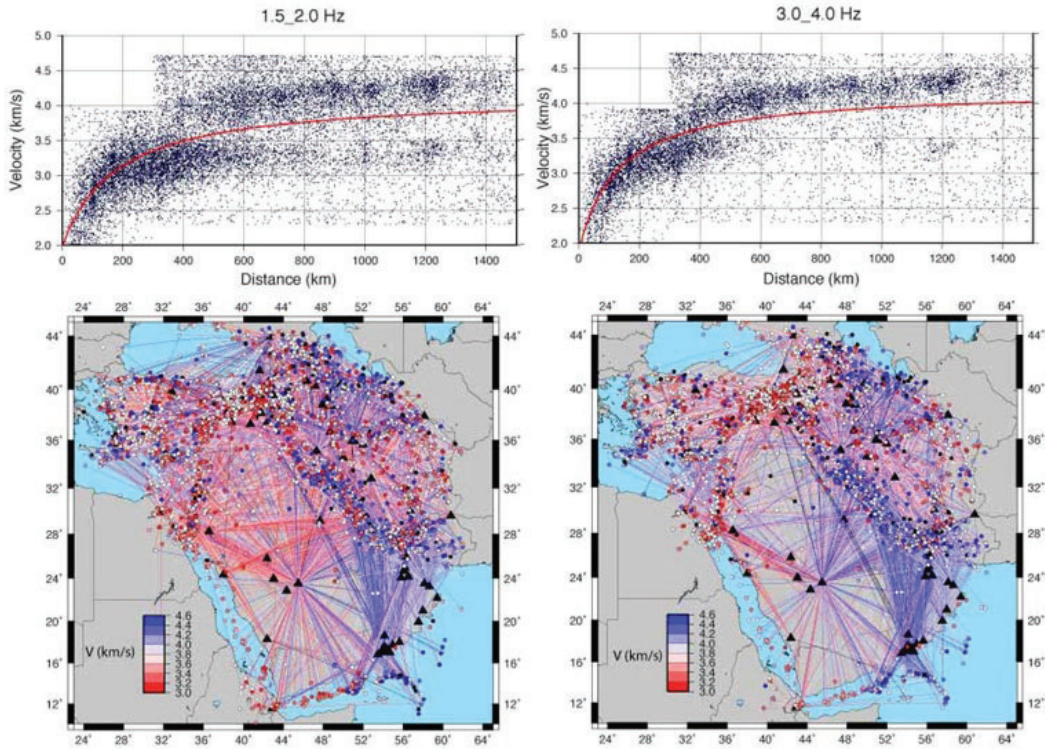

Figure 51. Variations in the velocities of the coda envelopes across the Middle East at four different frequency bands. *We see systematic variations in the velocity, and this variation is strongly frequency dependent.*

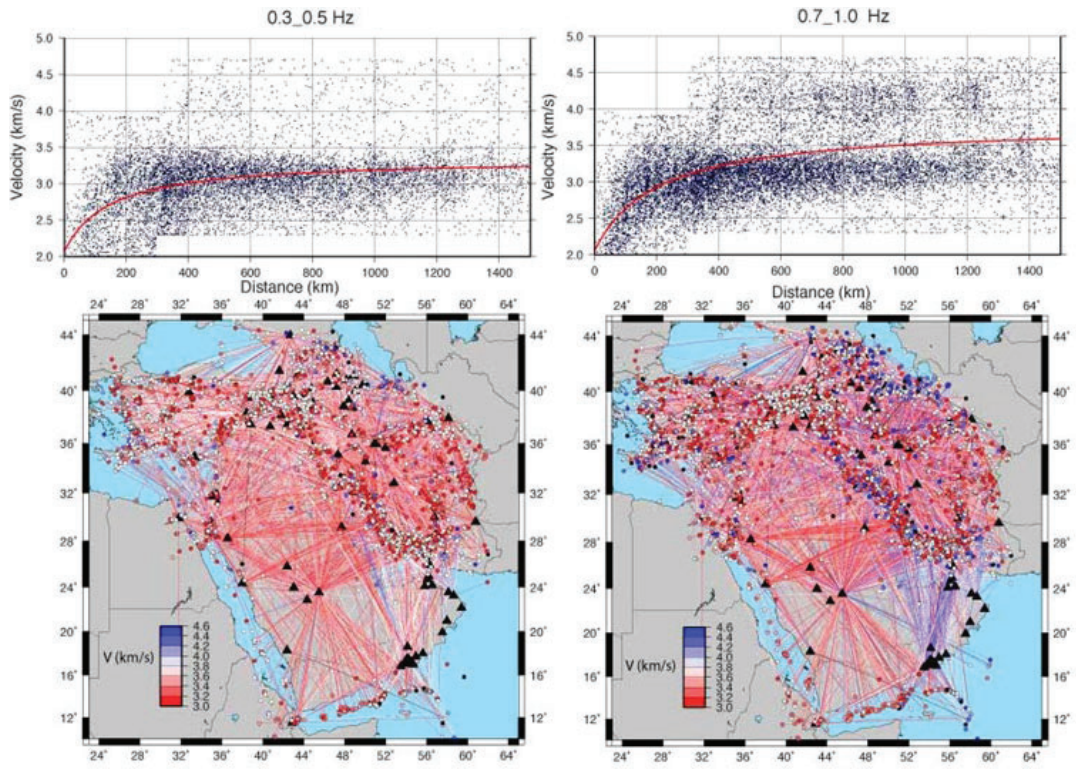

Figure 51 (continued). Variations in the velocities of the coda envelopes across the Middle East at four different frequency bands. *We see systematic variations in the velocity, and this variation is strongly frequency dependent.*

During the last year of the contract we began our analysis of coda stability. We use the coda amplitudes taken from the envelopes and investigate how these amplitudes change as a function of frequency between two different station pairs within the Iranian plateau (Figures 56 and 57).

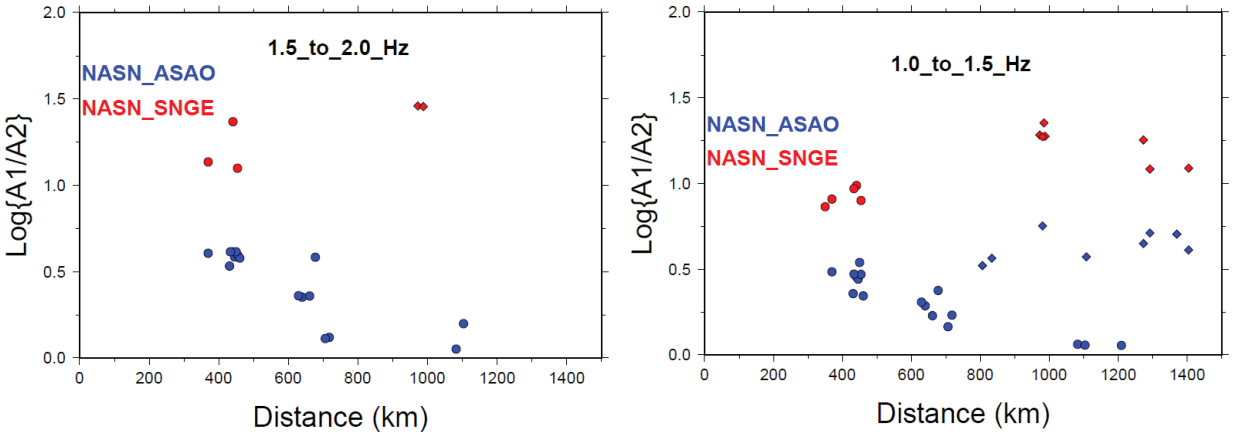

Figure 52. Two station ratio of coda amplitudes for a station pair within the Iranian plateau for a large combination of events approximately along the great circle path.

Using this approach, we found a great deal of scatter in the change in the coda amplitudes. The level of instability was similar to that observed in the direct wave amplitudes. Furthermore, we found more instability for some two-station pairs as compared with other stations located very near (northwestern Iranian plateau). The level of instability for these two-station pairs appears to be largely independent of frequency (Figure 52 compared with Figure 53). Of course, we need to analyze many more station pairs and to compare other coda parameters in addition to the coda amplitude.

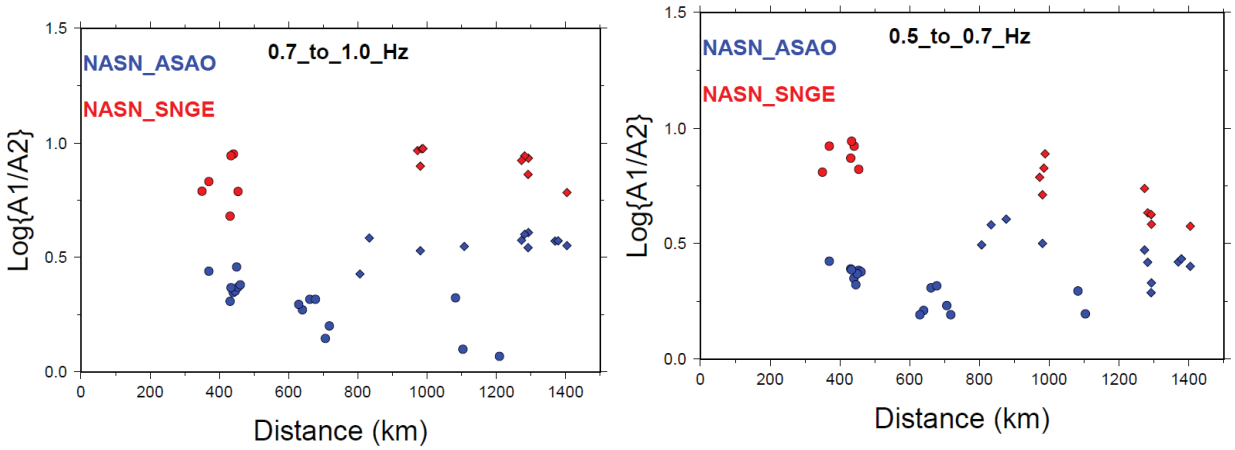

Figure 53. Two-station ratio of coda amplitudes, at lower frequencies than shown in Figure 52, for a station pair within the Iranian plateau for a large combination of events approximately along the great circle path.

5. CONCLUSIONS AND RECOMMENDATIONS

We have worked to fine tune our automated screening algorithms to explore the role that signal to noise ratio (SNR) plays in the Lg amplitude instabilities. Our investigations into the impact of pre-phase SNR on the stability of Lg Q estimates suggest that this was not the primary cause of amplitude instability in any of the sub-regions. Using tomographic maps of variance reductions with respect to pre-phase SNR both in time and in space, we are fairly sure that none of the instabilities that we have observed are principally a function of low SNR at any of the frequencies below 2 Hz. In summary, in our work on this contract we have seen pre-phase SNR making only very small differences in the tomographic models.

In this contract, we have processed existing and new data from the Middle East, Iran and the Caucasus combined seismic network (CNET) to help generate more RTS paths. We initially employed RTM data but this approach proved to be a little noisy, so the signals were not always clear enough to isolate the true cause of amplitude instability. However, once we started using the Two Station Method (TSM) method, the distance, depth, and temporal effects became fairly clear. Furthermore, our catalog of accurate relative depths from the Global Catalog of Calibrated Earthquake Locations and the Caucasus has helped us to successfully investigate Lg Q instability related to hypocentral depth and epicentral distance across the northern half of the Middle East. Furthermore, using the TSM

approach we found that there is not one single cause for the direct wave amplitude instability but that different factors appear to dominate in different regions (Figure 54). One of the key elements affecting high frequency wave amplitudes is the presence of a stable, cold lithospheric mantle. This is required for strong Sn propagation, which leads to leakage of energy from the lithospheric mantle wave guide into the crustal wave guide (Lg).

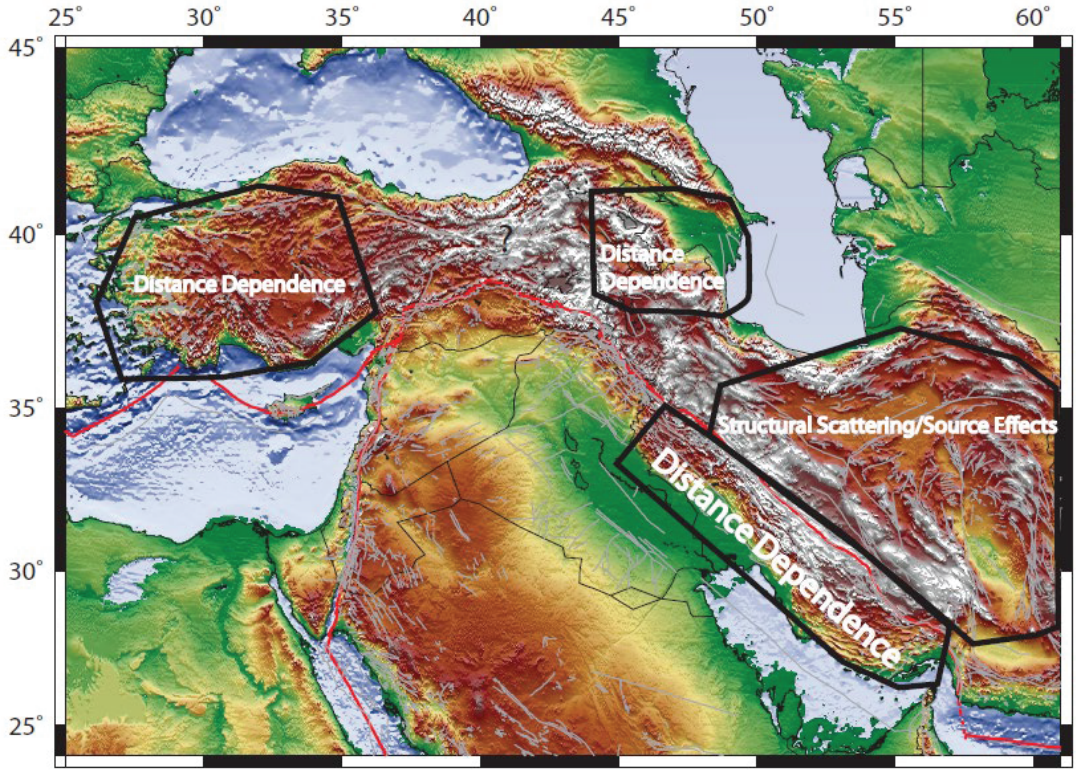

Figure 54. Summary figure showing what we have found to be the dominant effect(s) region by region. *It may be oversimplified, but it is mostly consistent with the effects we observed. We do not indicate a source for eastern Turkey because we did not find a clear cause for instability in that region.*

We finished preliminary work on examining instabilities in Lg Q using three-dimensional finite difference (SW4) modeling to look at differences in epicentral distance, source parameters, and azimuthal variations in site amplification. Our preliminary results seem to show a relatively clear distance dependence to the effective Lg Q. We have found that the effective Lg Q increased with distance, similar to what we observed in the Zagros and western Anatolian (Figure 54). One problem with our preliminary work might be a relatively high amount of numerical noise, although we seem to recover most of the crustal Q patterns when testing our synthetics. Furthermore, it is important to note, that more work on this issue likely needs to be done for much more complex seismic velocity structures.

Although in general we have not seen strong frequency dependence to the observed Lg amplitude instabilities, we have also a preliminary look at the frequency dependence of this type of distance and depth dependence and we have not found a great deal of change

from 2 to 0.5 Hz, although we only have completed some initial studies of the frequency dependence of the distance effect. We recommend for future work that the frequency dependence of the distance and source depth dependence is explored further.

REFERENCES

Baker, G.E., J. Stevens, and H. Xu, 2004, Lg group velocity: A depth discriminant revisited, *Bulletin of the Seismological Society of America*, 94 (2), pp. 722-739.

Chun, K.-Y., G. F. West, R. J. Kokoski, and C. Samson, 1987, A novel technique for measuring *Lg* attenuation-Results from eastern Canada between 1 to 10 Hz, *Bull. Seismol. Soc. Am.*, 77, pp. 398-419

Der, Z. A., M. E. Marshall, A. O'Donnell, and T. W. McElfresh, 1984, Spatial coherence structure and attenuation of the *Lg* phase, site effects, and the interpretation of the *Lg* coda, *Bull. Seismol. Soc. Am.*, 74, pp. 1125-1147.

Ford, S.R., D. S. Dreger, K. Mayeda, W. R. Walter, L. Malagnini, and W. W.Phillips, 2008, Regional attenuation in Northern California: A comparison of five 1D Q methods, *Bulletin of the Seismological Society of America*, 98 (4), pp. 2033-2046.

Gök, R.**,** A. Kaviani**,** E. M. Matzel, M. E. Pasyanos, K. Mayeda, G. Yetirmishli, I. El-Hussain, Al-Amri, F. Al-Jeri, T. Godoladze, D. Kalafat, E. A. Sandvol, and W. R. Walter, 2016, Moment Magnitudes of Local/Regional Events from 1-D Coda Calibrations in the Broader Middle East Region, *Bulletin of the Seismological Society of America, 106 (5), doi: 10.1785/0120160045*.

Kaviani, A., E. Sandvol, X. Bao, G. Rümpker, and R. Gök, 2015, The Structure of the Crust in the Turkish-Iranian Plateau and Zagros using Lg Q and Velocity, *Geophys. J. Int.*, 200 (2), pp. 1254-1268, doi: 10.1093/gji/ggu468.

Mayeda K., A. Hofstetter, J. L. O'Boyle., and W. R. Walter, 2003, Stable and transportable regional magnitudes based on coda-derived moment-rate spectra., *Bull. seismol. Soc. Am.*, 93, pp. 224-239.

Meunier, P., N. Hovius, and J. A. Haines, 2008, Topographic site effects and the location of earthquake induced landslides, *Earth Planet. Sci. Lett.*, 275, pp. 221-232, doi: 10.1016/j.epsl.2008.07.020.

Mitchell, B. J., 1995, Anelastic structure and evolution of the continental crust and upper mantle from seismic surface wave attenuation, *Rev. Geophys*., 33(4), pp. 441-462, doi:*10.1029/95RG02074*.

Motavalli-Anbaran, S.-H., H. Zeyen, and A. Jamasb, 2016, 3D crustal and lithospheric model of the Arabia-Eurasia collision zone*, Journal of Asian Earth Sciences*, 122, pp. 158-167.

Nuttli, O.W., 1980, The excitation and attenuation of seismic crustal phases in Iran, *Bull. Seismol. Soc. Am*. 70,pp. 469-485.

Paige, C.C. and M. A. Saunders, 1982, LSQR: An algorithm for sparse linear equations and sparse least squares, *ACM Trans. Math. Softw*. 8, pp. 43-71. http://dx.doi.org/10.1145/355984.355989.

Pasyanos, M. E., E. M. Matzel, W. R. Walter, and A. J. Rodgers, 2009, Broad-band *Lg* attenuation modelling in the Middle East, *Geophysical Journal International*, 177, pp. 1166-1176, doi: 10.1111/j.1365-246X.2009.04128.x.

Phillips, W. S., K. M. Mayeda, L. Malagnini, and C. A. Rowe, 2009, Developments in regional phase amplitude tomography, *Seism. Res. Lett.*, 80, 360.

Wald, D. J. and T. I. Allen, 2007, Topographic slope as a proxy for seismic site conditions and amplification, *Bull. Seismol. Soc. Am.*, 97, pp. 1379-1395, doi: 10.1785/0120060267.

Walter, W.R. and S.R. Taylor, 2001, A revised Magnitude and Distance Amplitude Correction (MDAC2) procedure for regional seismic discriminants: theory and testing at NTS, Lawrence Livermore National Laboratory, UCRL-ID-146882.

Xie, J. and B. J. Mitchell, 1990, A back-projection method for imaging large-scale lateral variations of Lg coda Q with application to continental Africa, *Geophys. J. Int*., 100, pp. 161-181, doi:10.1111/j.1365-246X.1990.tb02477.x.

Xie, J. 2002, Lg Q in the eastern Tibetan Plateau, *Bull. Seismol. Soc. Am*., 92, pp. 871-876, doi:10.1785/0120010154.

Xie, J., R. Gök, J. Ni, and Y. Aoki, 2004, Lateral variations of crustal seismic attenuation along the INDEPTH profiles in Tibet from *Lg Q* inversion, *J. Geophys. Res.*, 109, B10308, doi: 10.1029/2004JB002988.

Zabelina, I., I. Koulakov, I. Amanatashvili, I., S. El Khrepy, and N. Al-Arifi, 2016, Seismic structure of the crust and uppermost mantle beneath Caucasus based on regional earthquake tomography, *Journal of Asian Earth Science*s, 119, pp. 87-99.

List of Symbols, Abbreviations, and Acronyms

AFRL	Air Force Research Laboratory
CNET	Caucasus combined seismic NETwork
DTSM	Double Two Station Method
GCCE	Global Catalog of Calibrated Events
LLNL	Lawrence Livermore National Laboratory
MDAC	Magnitude and Distance Amplitude Correction
RTE	Reverse Two Event
RTM	Reverse Two Station Method
RTS	Reverse Two Station
SNR	Signal to Noise Ratio
TSCA	Two Station Coda Amplitude
TSM	Two Station Method

DISTRIBUTION LIST

DTIC/OCP
8725 John J. Kingman Rd, Suite 0944
Ft Belvoir, VA 22060-6218 1 cy

AFRL/RVIL
Kirtland AFB, NM 87117-5776 1 cy

Official Record Copy
AFRL/RVB/Dr. Frederick Schult 1 cy